Report

Cell Reports

Non-catalytic Roles of Tet2 Are Essential to Regulate Hematopoietic Stem and Progenitor Cell Homeostasis

Graphical Abstract

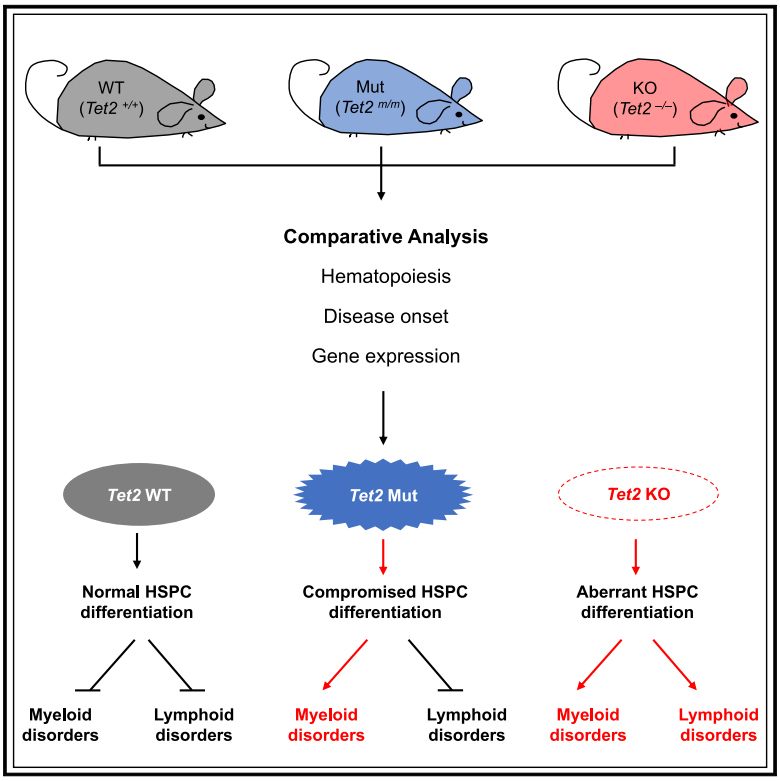

Highlights

- Loss of Tet2 enhances colony replating more than loss of its catalytic activity
- *Tet2* catalytic mutant mice predominantly develop myeloid malignancies
- *Tet2* knockout mice develop both myeloid and lymphoid disorders
- *Tet2* catalytic mutant versus knockout HSPCs exhibit distinct gene expression profiles

Authors

Kyoko Ito, Joun Lee, Stephanie Chrysanthou, ..., Deyou Zheng, Meelad M. Dawlaty, Keisuke Ito

Correspondence

meelad.dawlaty@einstein.yu.edu (M.M.D.), keisuke.ito@einstein.yu.edu (K.I.)

In Brief

The DNA demethylase *TET2* is commonly mutated in hematological disorders, but the significance of its enzymatic versus nonenzymatic roles in hematopoiesis remains undefined. Using *Tet2* catalytic-mutant and knockout mice, Ito et al. find that Tet2 enzymatic activity is critical for myelopoiesis, while aberrant lymphopoiesis is mainly associated with complete loss of *Tet2*.

Ito et al., 2019, Cell Reports *28*, 2480–2490
September 3, 2019
https://doi.org/10.1016/j.celrep.2019.07.094

CellPress

OPEN ACCESS
CellPress

Cell Reports
Report

Non-catalytic Roles of Tet2 Are Essential to Regulate Hematopoietic Stem and Progenitor Cell Homeostasis

Kyoko Ito,[1,2,3,7] Joun Lee,[1,4,7] Stephanie Chrysanthou,[1,4] Yilin Zhao,[4] Katherine Josephs,[1,4] Hiroyo Sato,[1,2,3] Julie Teruya-Feldstein,[6] Deyou Zheng,[4,5] Meelad M. Dawlaty,[1,4,8,*] and Keisuke Ito[1,2,3,8,9,*]

[1]Ruth L. and David S. Gottesman Institute for Stem Cell and Regenerative Medicine Research, Albert Einstein College of Medicine, 1301 Morris Park Ave., Bronx, NY 10461, USA
[2]Department of Cell Biology, Albert Einstein College of Medicine, 1300 Morris Park Ave., Bronx, NY 10461, USA
[3]Department of Medicine (Hemato-Oncology), Montefiore Medical Center, Albert Einstein College of Medicine, 1300 Morris Park Ave., Bronx, NY 10461, USA
[4]Department of Genetics, Albert Einstein College of Medicine, 1301 Morris Park Ave., Bronx, NY 10461, USA
[5]Departments of Neurology and Neuroscience, Albert Einstein College of Medicine, 1300 Morris Park Ave., Bronx, NY 10461, USA
[6]Department of Pathology, Icahn School of Medicine, Mount Sinai Health System, New York, NY USA
[7]These authors contributed equally
[8]Senior Author
[9]Lead Contact
*Correspondence: meelad.dawlaty@einstein.yu.edu (M.M.D.), keisuke.ito@einstein.yu.edu (K.I.)
https://doi.org/10.1016/j.celrep.2019.07.094

SUMMARY

The Ten-eleven translocation (TET) enzymes regulate gene expression by promoting DNA demethylation and partnering with chromatin modifiers. *TET2,* a member of this family, is frequently mutated in hematological disorders. The contributions of TET2 in hematopoiesis have been attributed to its DNA demethylase activity, and the significance of its nonenzymatic functions has remained undefined. To dissect the catalytic and non-catalytic requirements of Tet2, we engineered catalytically inactive *Tet2* mutant mice and conducted comparative analyses of *Tet2* mutant and *Tet2* knockout animals. *Tet2* knockout mice exhibited expansion of hematopoietic stem and progenitor cells (HSPCs) and developed myeloid and lymphoid disorders, while *Tet2* mutant mice predominantly developed myeloid malignancies reminiscent of human myelodysplastic syndromes. HSPCs from *Tet2* knockout mice exhibited distinct gene expression profiles, including downregulation of *Gata2*. Overexpression of *Gata2* in *Tet2* knockout bone marrow cells ameliorated disease phenotypes. Our results reveal the non-catalytic roles of TET2 in HSPC homeostasis.

INTRODUCTION

The Ten-eleven translocation (TET) family of dioxygenases (Tet1/2/3) are DNA-modifying enzymes expressed in various embryonic and adult cell types, including hematopoietic stem cells (HSCs) (Cimmino et al., 2011; Tahiliani et al., 2009). They regulate gene expression in part by promoting active and passive DNA demethylation through the conversion of 5-methylcytosine (5mC) to 5-hydroxymethylcytosine (5hmC) and other oxidized derivatives (Ito et al., 2010, 2011; Tahiliani et al., 2009). TET2 is a unique member of this family that is highly expressed in the hematopoietic lineages. It is one of the most frequently mutated genes in myelodysplastic syndrome (MDS), an incurable clonal hematological disorder marked by pronounced reductions in blood cell production, significant dysplasia in the cells produced, or some combination of both (Tefferi and Vardiman, 2009). Loss-of-function mutations in the *TET2* gene are seen in ~20% of MDS cases and almost 50% of chronic myelomonocytic leukemia (CMML) patients (Abdel-Wahab et al., 2009; Delhommeau et al., 2009; Kosmider et al., 2009; Song et al., 2013). While most mutations lead to loss of the entire protein, some are only missense mutations involving either the catalytic or non-catalytic domains (Abdel-Wahab et al., 2009; Sato et al., 2016). Deletion of *Tet2* in mice increases HSC self-renewal and restricts differentiation, causing CMML-like disease with aggressive metastases (Li et al., 2011; Moran-Crusio et al., 2011). In addition, loss of *TET2* has been linked to lymphoid disorders, as a fraction of *Tet2* knockout (KO) mice developed aberrant lymphopoiesis, and somatic mutations of *TET2* have been found in subtypes of lymphoid malignancies (e.g., angioimmunoblastic T lymphomas, ~33%; diffuse large B cell lymphomas, ~10%; and mantle cell lymphoma, 4%) (Asmar et al., 2013; Dominguez et al., 2018; Lemonnier et al., 2012; Mouly et al., 2018; Pan et al., 2017; Quivoron et al., 2011; Reddy et al., 2017).

The catalytic activity of Tet2 is mainly confined to its C terminus, which alone can promote DNA hydroxylation (Tahiliani et al., 2009). Tet2 has also been implicated in formation of chromatin regulatory complexes with O-linked N-acetylglucosamine transferase (OGT) and histone deacetylases (HDACs) to regulate transcription and histone modifications (Chen et al., 2013; Williams et al., 2011; Wu et al., 2011; Zhang et al., 2015). Thus far, the contributions of Tet2 to hematopoiesis have largely been studied using conventional or conditional KO mouse models

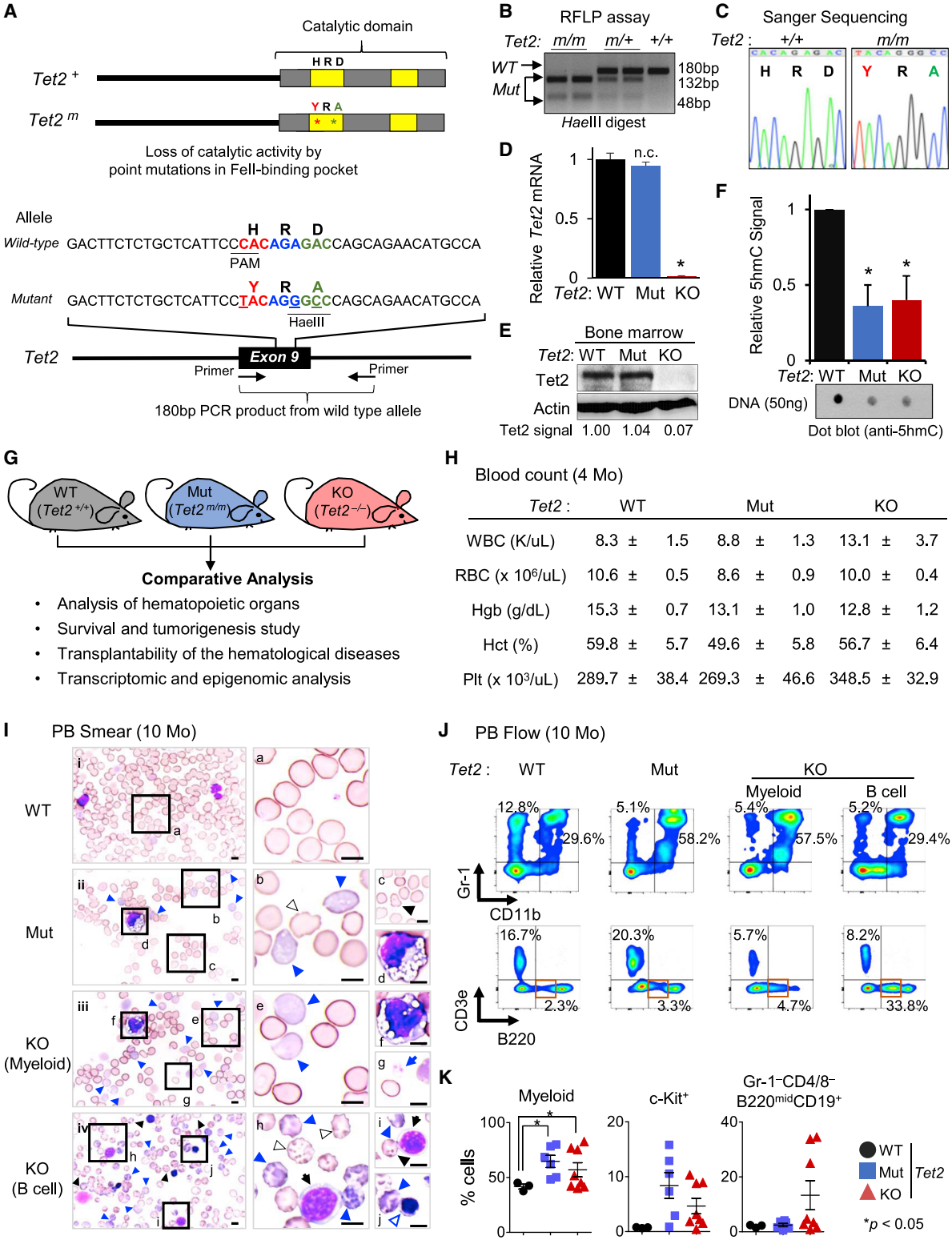

Blood count (4 Mo)	*Tet2* : WT	Mut	KO
WBC (K/uL)	8.3 ± 1.5	8.8 ± 1.3	13.1 ± 3.7
RBC (x 10^6/uL)	10.6 ± 0.5	8.6 ± 0.9	10.0 ± 0.4
Hgb (g/dL)	15.3 ± 0.7	13.1 ± 1.0	12.8 ± 1.2
Hct (%)	59.8 ± 5.7	49.6 ± 5.8	56.7 ± 6.4
Plt (x 10^3/uL)	289.7 ± 38.4	269.3 ± 46.6	348.5 ± 32.9

Figure 1. Generation of *Tet2* Catalytic Mutant (Mut) Mouse and Characterization of Its Hematological Phenotypes

(A) Tet2 wild-type (WT) and catalytic Mut proteins (top) and alleles (bottom).

(B and C) Analysis of the genotypes of *Tet2* catalytic Mut mice by RFLP (restriction fragment length polymorphism) (B) and Sanger sequencing (C).

(legend continued on next page)

that lack the entire Tet2 protein. Such an approach, despite interrogating the full functions of Tet2, fails to define or distinguish between its catalytic and non-catalytic requirements in a physiologically relevant context. In this study, to comprehensively dissect endogenous and physiologically relevant Tet2 functions during normal and abnormal hematopoiesis *in vivo*, we generated *Tet2* catalytically inactive mice by mutating the enzymatic pocket of the protein and conducted a comparative analysis of the resulting *Tet2* mutant (Mut) mice with *Tet2* KO mice. While both groups developed symptoms of hematological disorders early in life and had similar survival rates, differences in the disease spectrum were found between the cohorts; *Tet2* KO mice developed both myeloid and lymphoid disorders with increased hematopoietic stem and progenitor cell (HSPC) fractions. In contrast, in *Tet2* Mut mice, aberrant hematopoiesis was restricted largely to the myeloid lineage. Our study establishes that the role of Tet2 in hematopoietic system goes beyond its catalytic functions and identifies distinct non-catalytic requirements for Tet2 in the HSPC homeostasis, as well as in the onset of aberrant lymphopoiesis.

RESULTS

Generation of *Tet2* Catalytic Mut Mice

To establish the distinct contributions of catalytic functions of Tet2 to hematopoietic homeostasis, we developed a mouse strain lacking only the catalytic activity of Tet2. We generated a *Tet2* catalytic-deficient allele ($Tet2^{m}$) by introducing amino acid substitutions H1367Y and D1369A in the catalytic domain of Tet2 protein using CRISPR/Cas9-based gene editing in embryonic stem cells (ESCs) (Figure 1A). A properly targeted heterozygous $Tet2^{m/+}$ ESC clone was injected into blastocysts to generate chimeric mice (Figure S1A), which were bred to wild-type (WT) C57/BL6 mice to first generate $Tet2^{m/+}$ and then, after intercrossing, $Tet2^{m/m}$ mice (here after referred to as *Tet2* Mut) (Figures 1B and 1C). The *Tet2* Mut mice, like a previously used strain of $Tet2^{-/-}$ mice (*Tet2* KO) (Li et al., 2011), were born in expected Mendelian ratios and grew normally in a 129Sv-C57/BL6 mixed background (Figures S1B–S1D). The expression of *Tet2* was comparable in *Tet2* Mut and WT HSPCs ($Lin^{-}Sca\text{-}1^{+}c\text{-}Kit^{+}$ cells) at the mRNA level (Figure 1D) and in total bone marrow at the protein level (Figure 1E). 5hmC levels in DNA isolated from 2-month-old *Tet2* Mut bone marrow cells was reduced by ~60% and was similar to the level present in age-matched *Tet2* KO cells (Figure 1F). The *Tet2* KO mice lack all functions of the enzyme, while the *Tet2* Mut mice only lack the enzymatic activity of the protein. Therefore, *Tet2* Mut mice, in conjunction with *Tet2* KO and WT mice, comprise a viable platform for comparative physiological, cellular, and molecular analyses to dissect the catalytic-dependent and independent functions of Tet2 in HSPCs and MDS etiology (Figure 1G).

Analysis of Peripheral Blood of *Tet2* Mut Mice

At 4 months of age, *Tet2* Mut mice exhibited normal blood counts of the peripheral blood (PB) (Figure 1H). A trend of slightly higher white blood cell (WBC) counts was found in *Tet2* KO mice, but they had a normal range of red blood cell (RBC) and platelet counts (Figure 1H). Likewise, a mild increase in $CD11b^{+}$ cells was observed in *Tet2* KO mice, but flow cytometric analysis of PB revealed no significant dyspoiesis in either *Tet2* KO or *Tet2* Mut mice (Figure S1E).

At 10 months of age, *Tet2* Mut mice showed no significant blood count abnormalities (except for mild reductions in Hgb and Hct). In contrast, *Tet2* KO mice exhibited higher WBC counts with moderate anemia and lower platelet counts (data not shown). PB smear specimens revealed that *Tet2* Mut mice had multilineage dysplastic features, much like those found in human MDS (Giagounidis and Haase, 2013; Goasguen and Bennett, 1992; Komrokji et al., 2010; Wang, 2011). Dysplasia in monocytic lineages was predominant, but defective erythroid maturation and dysplastic platelets and neutrophils were also noted (Figures 1I and S1F). Flow cytometry analysis confirmed these myeloproliferative phenotypes in PB of *Tet2* Mut mice (Figures 1J, 1K, and S1G). As previously reported (Ko et al., 2011; Li et al., 2011; Moran-Crusio et al., 2011; Quivoron et al., 2011), one-third of *Tet2* KO mice developed human MDS-like phenotypes (Figures 1J and 1K; KO [myeloid]). However, in a few *Tet2* KO mice (<5%), a moderately increased frequency of $CD3e^{+}$ cells alone was the predominant phenotype (Figure S1H; KO [T cell]). Importantly, a significant portion (more than one-fourth) of *Tet2* KO

(D) *Tet2* mRNA levels in $Lin^{-}Sca\text{-}1^{+}c\text{-}Kit^{+}$ (LSK) cells of indicated genotypes quantified by qRT-PCR. Data are normalized to *Gapdh*. Note the absence of *Tet2* mRNA in knockout (KO) but its normal expression in Mut samples.

(E) Tet2 protein levels in total bone marrow isolated from 4-month-old mice assessed by western blot. Quantified Tet2 signal intensity normalized to actin signal intensity is shown. Note the absence of Tet2 protein in KO but its normal and comparable expression in Mut and WT samples.

(F) Levels of 5hmC in the bone marrow of the indicated genotypes, assessed by dot blot and quantified as average of three separated experiments (relative to WT control samples) (n = 3).

(G) Overview of experimental platform using *Tet2* WT, Mut, and KO mice.

(H) Blood counts of *Tet2* Mut and KO mice (4 months old, n = 8).

(I) Representative smears of peripheral blood (PB) of 10-month-old *Tet2* Mut (ii), *Tet2* KO with MDS-like myeloid (iii), and lymphoid (iv) phenotypes and WT control mice (i). Images of representative dysplastic hematopoietic cells found in *Tet2* Mut and KO mice are also shown (right; b–j, higher magnification images). *Tet2* Mut and KO mice show dysplastic erythroid cells (polychromatophilic, blue arrowhead; Howell-Jolly bodies, black arrowhead; other poikilocytes [e.g., echinocytes], outlined arrowhead; immature erythroid cells, blue-outlined arrowhead). Dysplastic myeloid cells (d and f) and dysplastic platelets (giant platelet, g), as well as immature B cells (black arrows [h and i]) are shown. All images are taken at ×100 magnification. Scale bars, 10 μm.

(J) Representative flow data for myeloid and lymphoid lineages in PB from *Tet2* Mut mice (middle) and *Tet2* KO mice with myeloid and B cell phenotypes (right) (10 months old). Flow data for WT control are also shown (left).

(K) Percentages ± SEM of $CD11b^{+}$ (left), $c\text{-}Kit^{+}$ (middle), and $B220^{low}CD19^{+}CD43^{+}$ (in $Gr\text{-}1^{-}CD4/8^{-}$ cells, right) cells in the PB in *Tet2* Mut (n = 6) and KO (n = 8) mice (10 months old).

Error bars indicate SD unless otherwise specified. n.c. stands for no significant change. See also Figure S1.

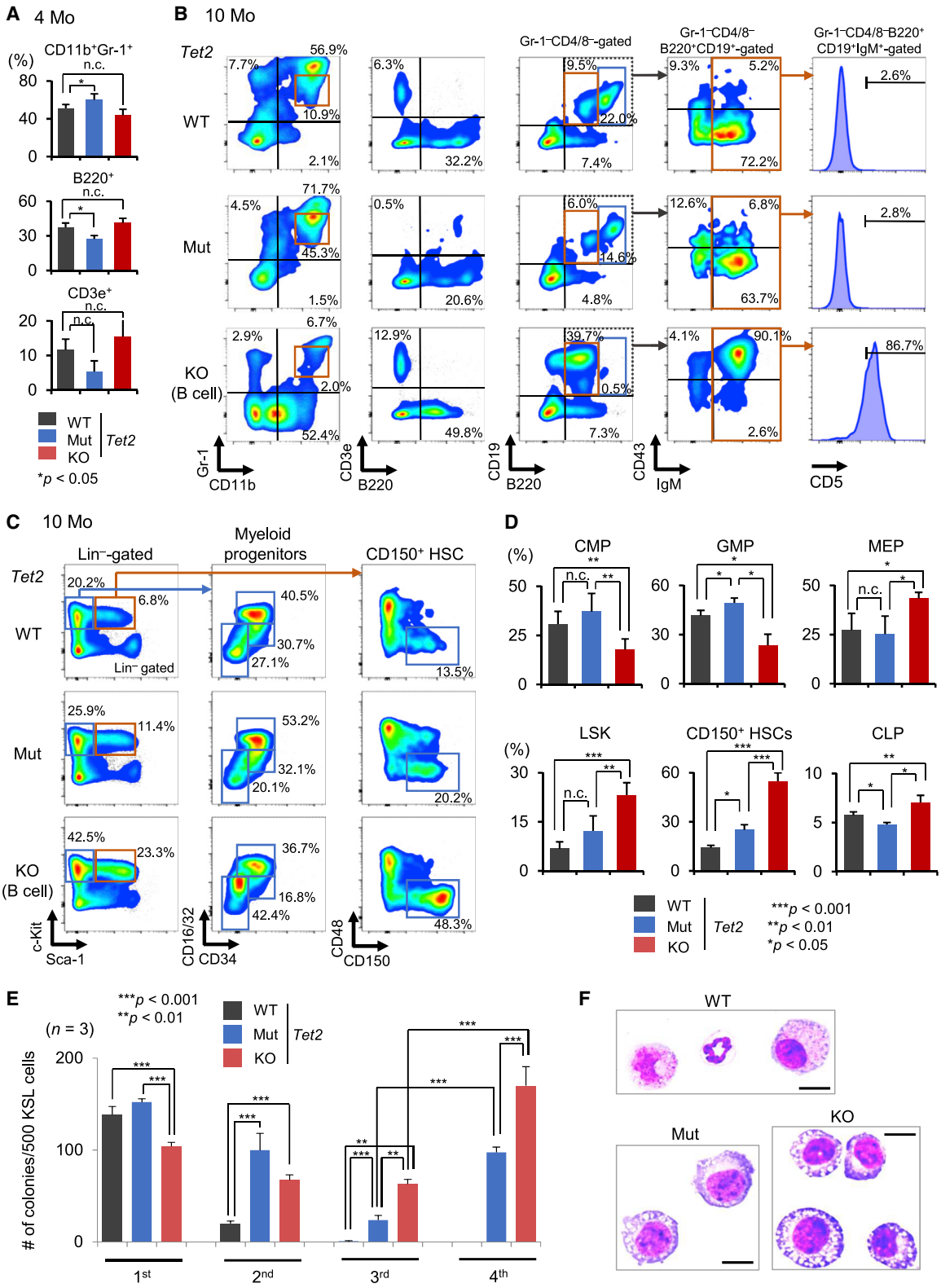

Figure 2. Analysis of *Tet2* Mut and KO Mouse Bone Marrow

(A) Percentages of the indicated fractions in the bone marrow of *Tet2* Mut and KO mice (4 months old) (n = 6).

(B) Bone marrow flow analysis for myeloid and lymphoid cells from *Tet2* Mut and KO mice (10 months old).

(legend continued on next page)

mice in study succumbed to aberrant lymphopoiesis, and these B cell phenotypes were more prevalent than dysplasia in myeloid or erythroid lineages (Figures 1J and 1K). Morphological analysis found immature forms of B lymphocytes in the PB of these mice. These were of small to medium size (cell diameter is 1.5–2 times that of an erythrocyte) and displayed scanty, round, and basophilic cytoplasm and clumped nuclear chromatin with relatively round nuclear outline, which are comparable morphological features to human chronic lymphocytic leukemia (CLL) or small lymphocytic lymphoma (SLL) (Figure 1I, KO [B cell] and Figure S1F, KO [lymphoid]). Flow cytometry assays showed an increase in $B220^{mid}$ cells, which are $CD19^{+}CD43^{+}$, implying defective differentiation in the B cell lineage (Figures 1J and 1K).

Characterization of Hematopoietic Phenotypes in *Tet2* Mut and *Tet2* KO Bone Marrow

At 4 months of age, *Tet2* Mut mice displayed a skewed myeloid/lymphoid ratio in the bone marrow (Figures 2A, S2A, and S2B). Similarly, *Tet2* KO mice with aberrant lymphopoiesis predominantly showed maturation defects in the B cell lineage, and these phenotypes became more striking with age (Figures 2B–2D, S2C, and S2D). Flow cytometric analysis of the bone marrow confirmed myeloproliferative phenotypes in 10-month-old *Tet2* Mut mice (Figures 2B and S2D). Notably, *Tet2* KO mice with myeloid disorders displayed similar myeloid proliferative phenotypes with analogous onset and severity (Figure S2D). In contrast, a portion of *Tet2* KO mice succumbed to B-lymphoid disorders, and a clear expansion of $Gr\text{-}1^{-}CD4/8^{-}B220^{mid}CD19^{+}CD43^{+}IgM^{+}$ abnormal B cells was observed in the bone marrow. These B cells reside in $CD5^{+}$, phenotypic B-1a lymphocytes, which have been suggested to relate to human CLL (Figure 2B; Yu et al., 2015). These defective B-1a homeostasis are consistent with the CLL-like morphological abnormalities in PB from *Tet2* KO mice (Figures 1K, 2B, and S2D).

The skewed myeloid/lymphoid ratio observed in bone marrow of *Tet2* Mut mice was also found at the progenitor stage; the myeloid-progenitor-enriched fractions ($Lin^{-}Sca1^{-}c\text{-}Kit^{+}$ cells) increased, while the lymphoid progenitors (common lymphoid progenitor [CLP]) were mildly decreased (Figures 2C, 2D, and S2C). MEP (megakaryocyte-erythroid progenitor) levels decreased and GMP (granulocyte-macrophage progenitor) levels increased in *Tet2* Mut mice (Figures 2C and 2D). *Tet2* KO mice with lymphoid phenotypes also displayed increased frequency of myeloid-progenitor-enriched fractions, but these increases were mainly attributed to higher numbers and frequency of MEPs. Common myeloid progenitor (CMP) levels decreased, while CLP levels were relatively maintained (Figures 2C and 2D). HSPCs were then analyzed. At 10 months, a higher number and frequency of LSK ($Lin^{-}Sca\text{-}1^{+}c\text{-}Kit^{+}$) cells and $CD135^{-}$LSK cells were found in *Tet2* KO mice, but not in *Tet2* Mut mice (Figures 2C, 2D, and S2D; data not shown). Furthermore, the frequency of HSC-enriched fractions ($CD150^{+}CD48^{-}CD135^{-}$LSK cells) increased in *Tet2* KO mice, regardless of having a myeloid or lymphoid phenotype (Figures 2C, 2D, and S2D).

These findings prompted us to subject HSPCs from 4-month-old WT, *Tet2* Mut, and KO mice to *in vitro* serial replating assay. We observed in the first plating that the *Tet2*-KO HSPCs produced fewer colonies compared to *Tet2* Mut or control cells, and a slightly increased ratio of macrophage colonies was found in *Tet2* Mut colonies (Figure S2E). However, after a third round of replating, *Tet2*-KO HSPCs exhibited increased colony-forming capacity compared to *Tet2* Mut and WT controls, and this phenotype was still pronounced in the next rounds of replating (Figure S2F). By 10 months of age, these phenotypes were even more evident; when *Tet2* Mut or KO colonies were replated, both *Tet2* Mut and KO cells produced more colonies in the second plating, and maintained this ability through serial replatings (Figures 2E and S2G). Notably, a comparison of third and fourth round of replating revealed that *Tet2*-KO HSPCs can produce a higher number of colonies than *Tet2*-Mut HSPCs (Figure 2E). Microscopic analysis of colonies formed after the second replating confirmed an increase in immature and dysplastic myeloid cells in *Tet2* Mut and KO colonies (Figures 2F and S2H). These analyses established that the non-catalytic functions of *Tet2* have distinct contributions to HSPC biology.

Distinct Disease Spectrum of *Tet2* Mut and KO Mice

Both *Tet2* Mut and KO mice exhibited splenomegaly and swollen lymph nodes, with an ~10-fold increase in spleen weight over age-matched controls (Figures 3A and 3B; not shown). The increased spleen sizes in *Tet2* Mut mice and in *Tet2* KO mice with myeloid phenotypes were attributed to myeloid infiltration (Figures 3C, 3D, and S3; data not shown). In *Tet2* KO mice with lymphoid phenotypes, immature B cells had increased in the spleen. Spleens were infiltrated with small to medium-sized, regular nuclear-contoured lymphoid cells in a diffuse pattern (Figures 3C, 3D, and S3). These phenotypes were even more evident at 10 months of age (Figures S3B and S3C).

Next, we compared the onset of hematological disorders and other signs of poor health in *Tet2* Mut with *Tet2* KO mice. The *Tet2* KO and *Tet2* Mut cohorts displayed similar overall survival, with 50% of animals dying by ~450 days and majority by ~800 days, while WT mice survived beyond 2 years (Figure 3E). Likewise, the two groups had similar incidence of

(C and D) Representative flow data for myeloid progenitors and HSPCs in the bone marrow from *Tet2* Mut and KO mice (10 months old). Percentages of the indicated fractions (percentage in $Lin^{-}Sca1^{-}c\text{-}Kit^{+}$ cells for CMPs, GMPs, and MEPs; percentage in $Lin^{-}CD127^{+}$ cells for CLPs; percentage in Lin^{-} cells for LSK; and percentage in $CD135^{-}$LSK cells for $CD150^{+}$ HSCs) (n = 6).

(E) *Tet2*-KO HSPCs have increased replating capacity compared to *Tet2*-Mut HSPCs (10 months old, up to fourth -round replating data) (n = 3).

(F) Representative images of May-Grünwald-Giemsa-stained cytospin preparations of the colonies formed by HSPCs from *Tet2* WT, Mut, and KO mice (at second replating). Metamyelocytes, myelocytes, and matured granulocytes consist of WT colonies, and immature and dysplastic myeloid cells are increased in *Tet2* Mut and KO colonies (also see Figure S2H). Scale bars, 10 μm.

HSPCs, hematopoietic stem and progenitor cells; LSK, $Lin^{-}c\text{-}Kit^{+}Sca\text{-}1^{+}$; MEP, megakaryocyte-erythrocyte progenitor, $Lin^{-}Sca\text{-}1^{-}c\text{-}Kit^{+}CD16/32^{low/neg}CD34^{low/neg}$; GMP, granulocyte-monocyte progenitor, $Lin^{-}Sca\text{-}1^{-}c\text{-}Kit^{+}CD16/32^{high}CD34^{+}$; CMP, common myeloid progenitor, $Lin^{-}Sca\text{-}1^{-}c\text{-}Kit^{+}CD16/32^{low}CD34^{+}$; CLP, common lymphoid progenitor, $Lin^{-}IL7R\alpha^{+}c\text{-}Kit^{mid}Sca\text{-}1^{+}$. Error bars indicate SD. n.c. stands for no significant change. See also Figure S2.

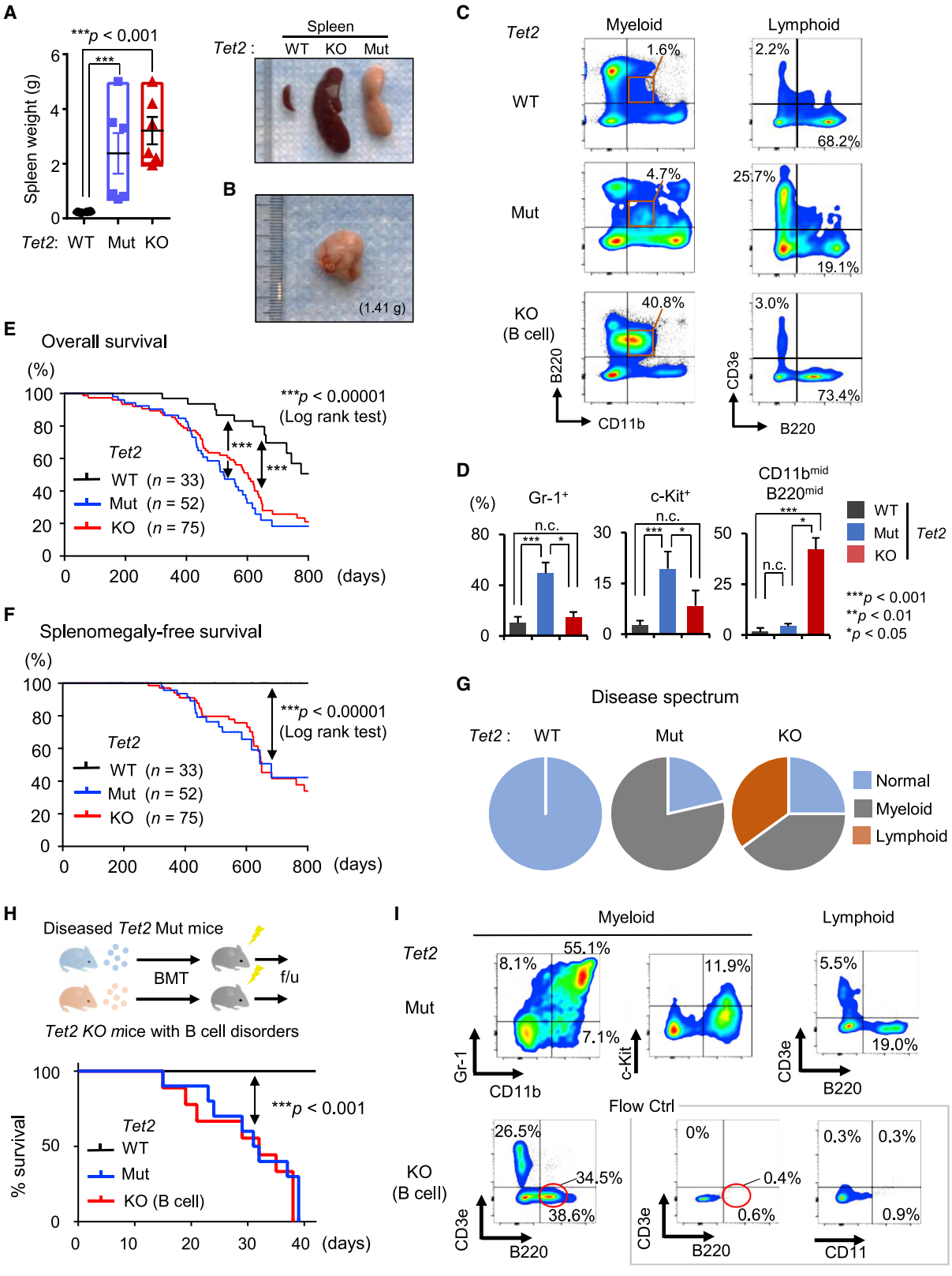

(legend on next page)

splenomegaly, and age-matched moribund *Tet2* Mut and KO mice had no significant differences in spleen size or weight (Figures 3A and 3F). However, most strikingly, despite the similar survival and disease onset of *Tet2* Mut and KO mice, the disease spectrum of *Tet2* Mut was different from that of *Tet2* KO mice: while *Tet2* KO mice developed both myeloid and lymphoid malignancies (44.4% and 38.9% [8/18 and 7/18], respectively), 78.5% (11/14) of *Tet2* Mut mice in our cohort displayed blood phenotypes restricted to the myeloid lineage by 10 months (Figure 3G).

These malignancies were readily transplantable. All recipient mice transplanted with *Tet2* Mut donor marrow cells initiated the lethal forms of myeloid disorders within 6 weeks (Figure 3H), and the resulting hematological phenotypes were similar to those observed in primary *Tet2* Mut mice. Monocyte-enriched $CD11b^+$ cells were increased, accompanied by dysplasia and c-Kit^+ myeloid blasts (Figure 3I; data not shown). Likewise, recipient mice transplanted with donor marrows from *Tet2* KO mice with B cell phenotypes developed lethal lymphoid disorders within 6 weeks, similar to the ones observed in primary *Tet2* KO mice (Figures 3H and 3I).

Distinct Gene Expression Changes in *Tet2* Mut versus KO HSPCs

To gain molecular insights into the catalytic and non-catalytic functions of Tet2 in HSPCs, we analyzed the gene expression profiles of 2-month-old *Tet2* Mut, *Tet2* KO and WT HSPCs (LSK) and Lin^- cells by RNA sequencing (RNA-seq) (Figure 4A–4F and S4A). We found 167 differentially expressed genes (DEGs) in *Tet2*-KO LSK (60 up, 107 down) compared to 568 DEGs in *Tet2*-Mut LSK cells (244 up, 344 down) (Figure 4A). Likewise, there were 197 DEGs in *Tet2*-KO Lin^- cells (106 up, 91 down) versus 180 DEGs in *Tet2*-Mut Lin^- cells (97 up, 83 down) (Figure 4D). Notably, in both LSK and Lin^- cells, most DEGs were changed by less than two fold, suggesting that in young progenitor cells gene expression changes due to either *Tet2* deficiency or loss of its catalytic activity are mostly subtle. However, comparison of the DEGs by clustering analysis (Figures 4B and 4E, left panels) or Venn diagrams (Figures 4B and 4E, right panels, and Figure S4B) revealed that the LSK and Lin^- cells from *Tet2* Mut and KO mice exhibited distinct gene expression profiles. Consistently, Gene Ontology enrichment analysis of DEGs in *Tet2* Mut and KO samples identified both common and distinct Gene Ontology (GO) terms, including cell proliferation, differentiation, gene regulation, and apoptosis (Figures 4C and 4F). This analysis suggests that complete loss of *Tet2* or loss of its catalytic activity alone leads to subtle but distinct changes in the gene expression programs of HSPCs.

Next, we integrated the RNA-seq data with the available Tet2 chromatin immunoprecipitation sequencing (ChIP-seq) datasets from WT mouse bone marrow (Deplus et al., 2013) and compared Tet2-bound genes with the list of DEGs. Approximately 50% of DEGs in *Tet2*-Mut and *Tet2*-KO LSK cells, as well as ~30% of DEGs in *Tet2*-Mut and *Tet2*-KO Lin^- cells, were bound by Tet2 (i.e., direct targets of Tet2) (Figures 4G and S4C). Classification of Tet2 peak location at these direct target genes revealed that over 80% of Tet2 binding occurred at promoters (Figure 4H). These genes with Tet2 binding at promoters included several regulators of HSCs and lineage specifiers. Among them, two transcription factors, *Hoxa9* and *Gata2*, were significantly downregulated in *Tet2*-KO, but not in *Tet2*-Mut, LSK, or Lin^- cells, respectively (Figure 4I). Other regulators of HSCs such as *Gata1* and *Spi1* were not affected, while *Tet1* was downregulated in both *Tet2*-Mut and *Tet2*-KO LSK cells, and *Tet3* expression was marginally reduced in *Tet2*-KO LSK cells (Figure S4D). Next, we examined whether the reexpression of selected identified downstream effectors of non-catalytic roles of Tet2, such as Gata2, can rescue disease phenotypes observed in *Tet2* KO mice. *Gata2* overexpression in *Tet2* KO bone marrow cells ameliorated lymphoid disease phenotypes and conferred significant survival advantage (Figures 4J, 4K, S4E, and S4F). However, in *Tet2* Mut bone marrow cells, it failed to rescue myeloid phenotypes (Figure 4K). Collectively, our findings suggest that the Tet2 catalytic activity primarily regulates the myeloid lineage, while its non-catalytic functions modulate the lymphoid lineage. As such, loss of Tet2 enzymatic activity alone predominantly leads to myeloid malignancies, while complete loss of *Tet2* influences the hemostasis of both myeloid and lymphoid lineages, leading to aggressive malignancies of cell types of both lineages (Figure 4L).

DISCUSSION

Tet2 loss causes progressive defects in hematopoiesis, such as increased HSC self-renewal, and has been implicated in both myeloid and lymphoid disorders (Asmar et al., 2013; Dominguez et al., 2018; Lemonnier et al., 2012; Mouly et al., 2018; Pan et al., 2017; Quivoron et al., 2011; Reddy et al., 2017). The analysis of our cohorts of *Tet2* Mut and KO mice have provided three lines of evidence that together establish the biological requirements

Figure 3. Characterization of Hematological Malignancies in *Tet2* Catalytic Mut Mice

(A and B) Spleen weight (n = 3–6; A, left). Representative images of spleens from *Tet2* Mut mice with myeloid phenotypes and *Tet2* KO mice with lymphoid phenotypes (A, right) (10 months old). Representative images of lymph nodes from *Tet2* Mut mice with myeloid phenotypes (B).

(C and D) Representative flow data for myeloid and lymphoid lineages in spleens from *Tet2* Mut mice with myeloid phenotypes (C, middle) and *Tet2* KO mice with lymphoid phenotypes (C, bottom) (10 months old). The percentages of indicated fractions in spleens from *Tet2* Mut and *Tet2* KO mice are shown (D, n = 6).

(E and F) Kaplan-Meier survival curves of overall survival (E) and splenomegaly-free survival (F) of *Tet2* Mut and KO mice. The number of mice in each group are shown in parenthesis. Log-rank test was used to generate p values.

(G) Disease spectrum in *Tet2* Mut and KO mice (n = 16, 18, respectively).

(H and I) Schematic of transplantation of diseased bone marrow (H, top). Survival curve of transplanted mice (H, bottom, n = 10 for Mut, 9 for WT and KO). All recipient mice transplanted with *Tet2* Mut bone marrow developed lethal myeloid malignancies within 6 weeks after bone marrow transplantation (BMT) (H, bottom). Representative flow cytometric analysis for myeloid and lymphoid lineages in PB of recipient mice transplanted with *Tet2* Mut (I. top) or KO (I. bottom) bone marrow, 3 weeks after BMT are shown.

Error bars indicate SD. n.c. stands for no significant change. See also Figure S3.

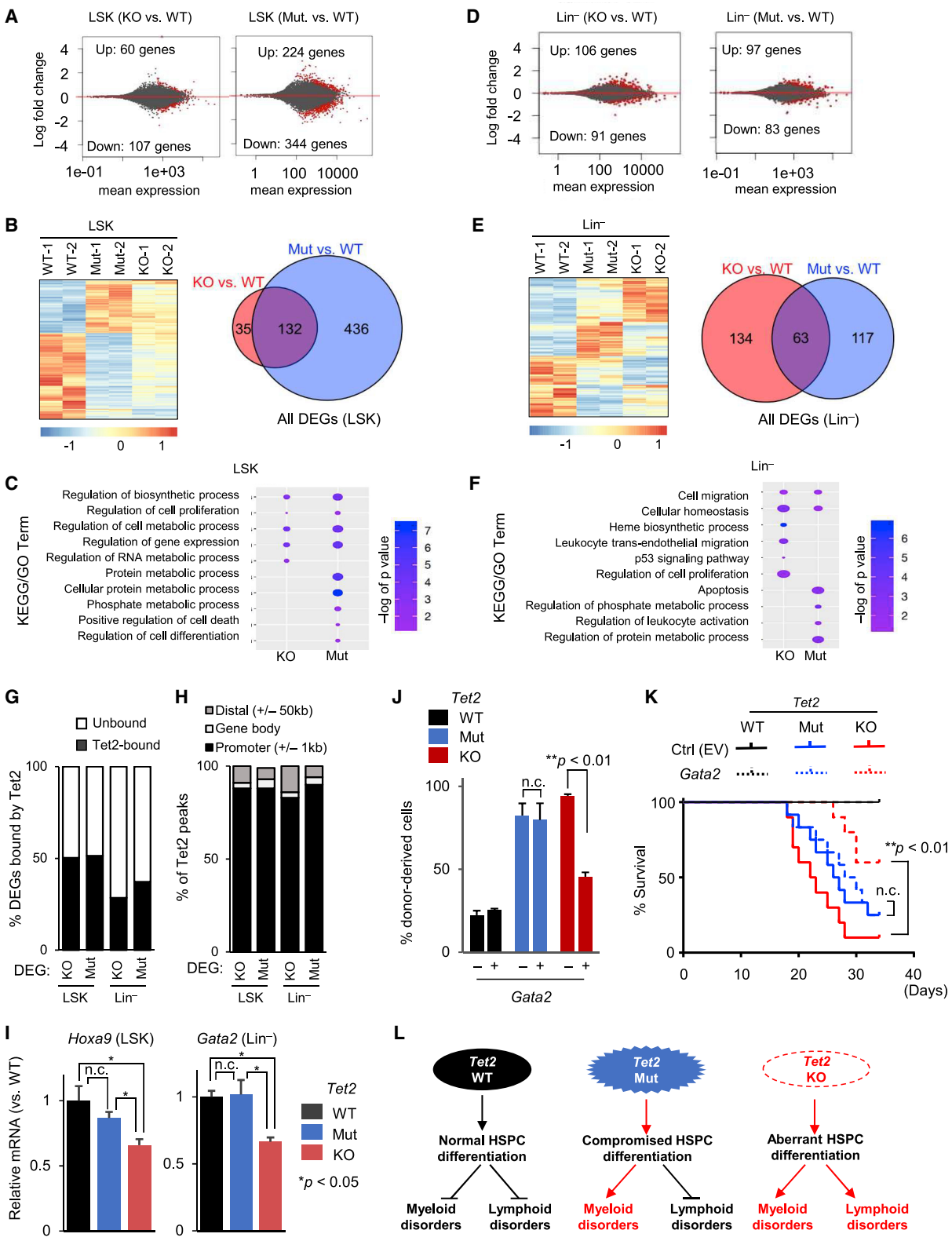

Figure 4. Gene Expression Profiling of *Tet2* Mut and KO HSPCs

(A) MA plot of RNA-seq analysis of 2-month-old LSK cells as log2 fold change versus mean gene expression levels. Differentially expressed genes (DEGs) are depicted in red. Mut or KO groups are compared to WT.

(legend continued on next page)

of the non-catalytic functions of Tet2 to HSPC maintenance and tumor suppression: (1) loss of *Tet2*, compared to loss of its catalytic activity alone, leads to greater expansion of HSPCs and enhanced colony formation; (2) *Tet2* Mut mice predominantly develop myeloid malignancies, while *Tet2* KO mice develop both myeloid and lymphoid disorders; and (3) despite similar 5hmC levels, *Tet2*-KO and *Tet2*-Mut HSPCs have different gene expression profiles, and *Tet2*-KO HSPCs express reduced levels of HSC lineage specifiers *Gata2* and *Hoxa9*. These findings provide conceptual advances to our understanding of requirements of Tet2 in hematopoiesis. The current dogma primarily attributes the contributions of Tet2 in HSPCs and hematological disorders to its enzymatic or DNA demethylase activity (Li et al., 2011; Moran-Crusio et al., 2011; Quivoron et al., 2011; Tahiliani et al., 2009). Our work shifts this "paradigm" by associating the catalytic and non-catalytic roles of Tet2 to distinct disease etiologies involving the myeloid and lymphoid lineages, respectively.

Increased incidence of aberrant lymphopoiesis is a distinct feature of *Tet2* loss that is not seen in *Tet2* Mut mice, suggesting that Tet2 non-catalytic roles are involved in regulation of lymphopoiesis. Interestingly, ~30% of *Tet2* KO mice showed the accumulation of phenotypic B-1a lymphocytes, $B220^{low}CD19^{+}IgM^{+}CD43^{+}CD11b^{low}CD5^{+}$ cells, and developed B cell neoplasms that are comparable to human CLL. We note that mantle cell lymphoma is also a $CD5^{+}$ B cell neoplasm, and the abnormal B cells found in *Tet2* KO mice are $CD23^{mid}$ positive (Figure S3B). However, these cells showed no *Ccnd1* upregulation (data not shown), and the pathological and morphological features observed in *Tet2*-loss-induced neoplasms classify them as a CLL-like disorder. Intriguingly, *TET2* mutations are rare (~2.3%) in human CLL, but there are also several reports of loss of *TET2* function in B cell lymphomagenesis with blockade of plasma cell differentiation (Asmar et al., 2013; Dominguez et al., 2018; Lemonnier et al., 2012; Mouly et al., 2018; Pan et al., 2017; Quivoron et al., 2011; Reddy et al., 2017).

Establishing the mechanisms by which *Tet2* deficiency leads to diverse hematological abnormalities is critical for understanding how Tet2 regulates normal hematopoiesis and how its downregulation or mutations as seen in various cancers contribute to tumorigenesis. This is of paramount significance in therapeutic strategies for hematological disorders involving loss of *TET2*. Analysis of our *Tet2* Mut mouse model conclusively establishes that the catalytic activity of Tet2 is the prime regulator of myeloid lineage and MDS pathogenesis. This suggests that Tet2 targets affected in MDS are regulated by the enzymatic activity of Tet2 through DNA demethylation. Consistently, DNA hypermethylation is a hallmark of hematologic disorders, and DNA demethylating agents such as 5-Aza-2′-deoxycytidine (decitabine) are used to treat higher-risk MDS and acute myeloid leukemia (Fabiani et al., 2010; Garcia-Manero and Fenaux, 2011; Gardin and Dombret, 2017; Issa et al., 2004). Likewise, vitamin C (which boosts TET enzymatic activity) has been shown to be of therapeutic benefit in MDS and CMML disease in mice haploinsufficient for *Tet2* (Agathocleous et al., 2017; Cimmino et al., 2017). Since our model attributes regulation of lymphopoiesis and suppression of lymphomagenesis to the non-catalytic roles of Tet2, it is likely that such treatments might not be as effective in *TET2*-loss-driven lymphoid disorders. Here, we identify key transcription factors and lineage specifiers *Hoxa9* and *Gata2* as direct targets of Tet2 that are deregulated in *Tet2* KO, but not *Tet2* Mut, HSPCs. We have shown that *Gata2* can rescue lymphoid-associated phenotypes observed in *Tet2* KO mice. Further work will determine how these genes are regulated in a Tet2 catalytic-independent manner, possibly involving OGT and or HDAC2 (Chen et al., 2013; Zhang et al., 2015). Identification of additional catalytic and non-catalytic targets and mechanisms of Tet2 that are distinctly associated with myeloid versus lymphoid diseases will further enhance our understanding of how TET2 contributes to HSPC maintenance and suppresses hematological disorders and malignancies. This will substantially impact strategies for how TET2 should be targeted for therapeutic purposes.

STAR★METHODS

Detailed methods are provided in the online version of this paper and include the following:

- KEY RESOURCES TABLE
- LEAD CONTACT AND MATERIALS AVAILABILITY

(B) Heatmap of differentially expressed genes identified by RNA-seq across LSK cells of indicated genotypes. Genes differentially expressed in at least one of the comparisons are displayed. Intensity values are log2 transformed (left) and colors represent relative expression across samples. Venn diagram illustrating the overlap between all DEGs in *Tet2*-Mut and *Tet2*-KO LSK cells (right).
(C) Selected terms from GO and KEGG analysis of DEGs in LSK cells. Data are plotted with colors for −log10 of p value and bubble sizes for numbers of genes.
(D) MA plot of RNA-seq analysis of 2-month-old Lin^{-} cells as log2 fold change versus mean gene expression levels. DEGs are depicted in red (compared to WT).
(E) Heatmap (left) of DEGs identified by RNA-seq across Lin^{-} cells of indicated genotypes. Genes differentially expressed in at least one of the comparisons are displayed. Venn diagram illustrating the overlap between all DEGs in *Tet2*-Mut and *Tet2*-KO Lin^{-} cells (right).
(F) Selected terms from GO and KEGG analysis of DEGs in Lin^{-} cells. Data are plotted with colors for −log10 of p value and bubble sizes for numbers of genes.
(G) Comparison of DEGs with Tet2 ChIP-seq peaks in bone marrow, revealing that nearly half of DEGs in LSK cells and approximately one-third of DEGs in Lin^{-} cells are bound by Tet2 (i.e., direct targets of Tet2). Tet2 ChIP-seq data were from a previous study (see STAR Methods)
(H) Classification of Tet2 peaks at DEGs revealing that Tet2 binding is enriched at the promoters of Tet2-bound DEGs.
(I) Relative expression levels of *Hoxa9* and *Gata2* mRNA in LSK or Lin^{-} cells from mice of indicated genotypes (compared to WT control samples), quantified by qRT-PCR (n = 3). Data normalized to *Gapdh*.
(J and K) Overexpression of *Gata2* in the bone marrow of *Tet2* Mut or KO mice with MDS- or CLL-like hematopoietic disorder, respectively, followed by competitive BMT (mixture of test cells [Ly45.2] with competitor [Ly45.1/45.2] in a 1:3 ratio). Percentage of donor-derived cells in PB of recipient mice transplanted 3 weeks after BMT is shown in (J) (n = 4), and the survival curve of transplanted mice is shown in (K) (n = 8, 12, and 10 for WT, Mu, and KO, respectively).
(L) Model summarizing the effects of loss of *Tet2* versus loss of its catalytic activity alone on myeloid and lymphoid lineage homeostasis and development of malignancies.
Error bars indicate SD. n.c. stands for no significant change. See also Figure S4.

SUPPLEMENTAL INFORMATION

Supplemental Information can be found online at https://doi.org/10.1016/j.celrep.2019.07.094.

ACKNOWLEDGMENTS

We thank the Einstein epigenomics, flow cytometry (NIH grant P30 CA013330), histopathology, and transgenic cores for help with RNA-seq, cell sorting, sectioning tissues, and blastocyst injections, respectively. We are grateful to M. Xu for the *Tet2* knockout mouse strain and M. Yoshimoto for the critical discussions of B lymphopoiesis. We thank Q. Tang and other members of the Ito and Dawlaty labs, as well as P.S. Frenette, U. Stiedl, A. Verma, and other members of Einstein Stem Cell Institute, for helpful suggestions and discussions. M.M.D. is supported by the Sidney Kimmel Foundation, the Leukemia Research Foundation, NYSDOH/NYSTEM, and the NIH NIGMS (grant R01GM122839). Keisuke Ito is supported by the NIH NIDDK (grants R01DK98263, R01DK115577, and R01DK100689) and NYSDOH as core director of Einstein single-cell genomics/epigenomics (C029154). M.M.D. and Keisuke Ito are also supported by funds from the Ruth L. and David S. Gottesman Institute for Stem Cell and Regenerative Medicine Research at Einstein, as well as by the NIH NHLBI (grant R01HL148852 to M.M.D. and Keisuke Ito as multi-PIs). S.C. is supported by the Einstein Training Program in Stem Cell Research from the Empire State Stem Cell Fund (C30292GG). Y.Z. and D.Z. are in part supported by the NIH NEI (grants R01 EY014237 and EY012200). Keisuke Ito is a Scholar of The Leukemia and Lymphoma Society (#1360-19).

AUTHOR CONTRIBUTIONS

Kyoko Ito performed analyses of hematopoietic tissues and their function. J.L. and K.J. established and monitored mouse cohort study and performed necropsy. Kyoko Ito and J.L. carried out histology and J.T.-F. performed pathological analyses. Y.Z. and D.Z. analyzed the RNA-seq and ChIP-seq data. H.S. provided technical support. S.C. supported the molecular analyses. M.M.D. and Keisuke Ito designed the study, supervised execution of experiments, secured funding, and wrote the manuscript with input from other authors.

DECLARATION OF INTERESTS

The authors declare no competing interests.

Received: December 31, 2018
Revised: June 11, 2019
Accepted: July 24, 2019
Published: September 3, 2019

REFERENCES

Abdel-Wahab, O., Mullally, A., Hedvat, C., Garcia-Manero, G., Patel, J., Wadleigh, M., Malinge, S., Yao, J., Kilpivaara, O., Bhat, R., et al. (2009). Genetic characterization of TET1, TET2, and TET3 alterations in myeloid malignancies. Blood *114*, 144–147.

Agathocleous, M., Meacham, C.E., Burgess, R.J., Piskounova, E., Zhao, Z., Crane, G.M., Cowin, B.L., Bruner, E., Murphy, M.M., Chen, W., et al. (2017). Ascorbate regulates haematopoietic stem cell function and leukaemogenesis. Nature *549*, 476–481.

Anders, S., Pyl, P.T., and Huber, W. (2015). HTSeq—a Python framework to work with high-throughput sequencing data. Bioinformatics *31*, 166–169.

Asmar, F., Punj, V., Christensen, J., Pedersen, M.T., Pedersen, A., Nielsen, A.B., Hother, C., Ralfkiaer, U., Brown, P., Ralfkiaer, E., et al. (2013). Genome-wide profiling identifies a DNA methylation signature that associates with TET2 mutations in diffuse large B-cell lymphoma. Haematologica *98*, 1912–1920.

Chen, Q., Chen, Y., Bian, C., Fujiki, R., and Yu, X. (2013). TET2 promotes histone O-GlcNAcylation during gene transcription. Nature *493*, 561–564.

Cimmino, L., Abdel-Wahab, O., Levine, R.L., and Aifantis, I. (2011). TET family proteins and their role in stem cell differentiation and transformation. Cell Stem Cell *9*, 193–204.

Cimmino, L., Dolgalev, I., Wang, Y., Yoshimi, A., Martin, G.H., Wang, J., Ng, V., Xia, B., Witkowski, M.T., Mitchell-Flack, M., et al. (2017). Restoration of TET2 function blocks aberrant self-renewal and leukemia progression. Cell *170*, 1079–1095.e1020.

Delhommeau, F., Dupont, S., Della Valle, V., James, C., Trannoy, S., Massé, A., Kosmider, O., Le Couedic, J.P., Robert, F., Alberdi, A., et al. (2009). Mutation in TET2 in myeloid cancers. N. Engl. J. Med. *360*, 2289–2301.

Deplus, R., Delatte, B., Schwinn, M.K., Defrance, M., Méndez, J., Murphy, N., Dawson, M.A., Volkmar, M., Putmans, P., Calonne, E., et al. (2013). TET2 and TET3 regulate GlcNAcylation and H3K4 methylation through OGT and SET1/COMPASS. EMBO J. *32*, 645–655.

Dominguez, P.M., Ghamlouch, H., Rosikiewicz, W., Kumar, P., Béguelin, W., Fontán, L., Rivas, M.A., Pawlikowska, P., Armand, M., Mouly, E., et al. (2018). TET2 deficiency causes germinal center hyperplasia, impairs plasma cell differentiation, and promotes B-cell lymphomagenesis. Cancer Discov. *8*, 1632–1653.

Fabiani, E., Leone, G., Giachelia, M., D'alo', F., Greco, M., Criscuolo, M., Guidi, F., Rutella, S., Hohaus, S., and Voso, M.T. (2010). Analysis of genome-wide methylation and gene expression induced by 5-aza-2′-deoxycytidine identifies BCL2L10 as a frequent methylation target in acute myeloid leukemia. Leuk. Lymphoma *51*, 2275–2284.

Garcia-Manero, G., and Fenaux, P. (2011). Hypomethylating agents and other novel strategies in myelodysplastic syndromes. J. Clin. Oncol. *29*, 516–523.

Gardin, C., and Dombret, H. (2017). Hypomethylating agents as a therapy for AML. Curr. Hematol. Malig. Rep. *12*, 1–10.

Giagounidis, A., and Haase, D. (2013). Morphology, cytogenetics and classification of MDS. Best Pract. Res. Clin. Haematol. *26*, 337–353.

Goasguen, J.E., and Bennett, J.M. (1992). Classification and morphologic features of the myelodysplastic syndromes. Semin. Oncol. *19*, 4–13.

Issa, J.P., Garcia-Manero, G., Giles, F.J., Mannari, R., Thomas, D., Faderl, S., Bayar, E., Lyons, J., Rosenfeld, C.S., Cortes, J., and Kantarjian, H.M. (2004). Phase 1 study of low-dose prolonged exposure schedules of the hypomethylating agent 5-aza-2′-deoxycytidine (decitabine) in hematopoietic malignancies. Blood *103*, 1635–1640.

Ito, S., D'Alessio, A.C., Taranova, O.V., Hong, K., Sowers, L.C., and Zhang, Y. (2010). Role of Tet proteins in 5mC to 5hmC conversion, ES-cell self-renewal and inner cell mass specification. Nature *466*, 1129–1133.

Ito, S., Shen, L., Dai, Q., Wu, S.C., Collins, L.B., Swenberg, J.A., He, C., and Zhang, Y. (2011). Tet proteins can convert 5-methylcytosine to 5-formylcytosine and 5-carboxylcytosine. Science *333*, 1300–1303.

Ito, K., Carracedo, A., Weiss, D., Arai, F., Ala, U., Avigan, D.E., Schafer, Z.T., Evans, R.M., Suda, T., Lee, C.H., and Pandolfi, P.P. (2012). A PML–PPAR-δ pathway for fatty acid oxidation regulates hematopoietic stem cell maintenance. Nat. Med. *18*, 1350–1358.

Ito, K., Turcotte, R., Cui, J., Zimmerman, S.E., Pinho, S., Mizoguchi, T., Arai, F., Runnels, J.M., Alt, C., Teruya-Feldstein, J., et al. (2016). Self-renewal of a purified Tie2+ hematopoietic stem cell population relies on mitochondrial clearance. Science *354*, 1156–1160.

Jiao, X., Sherman, B.T., Huang da, W., Stephens, R., Baseler, M.W., Lane, H.C., and Lempicki, R.A. (2012). DAVID-WS: a stateful web service to facilitate gene/protein list analysis. Bioinformatics *28*, 1805–1806.

Kim, D., Pertea, G., Trapnell, C., Pimentel, H., Kelley, R., and Salzberg, S.L. (2013). TopHat2: accurate alignment of transcriptomes in the presence of insertions, deletions and gene fusions. Genome Biol. *14*, R36.

Ko, M., Bandukwala, H.S., An, J., Lamperti, E.D., Thompson, E.C., Hastie, R., Tsangaratou, A., Rajewsky, K., Koralov, S.B., and Rao, A. (2011). Ten-Eleven-Translocation 2 (TET2) negatively regulates homeostasis and differentiation of hematopoietic stem cells in mice. Proc. Natl. Acad. Sci. USA *108*, 14566–14571.

Komrokji, R.S., Zhang, L., and Bennett, J.M. (2010). Myelodysplastic syndromes classification and risk stratification. Hematol. Oncol. Clin. North Am. *24*, 443–457.

Kosmider, O., Gelsi-Boyer, V., Ciudad, M., Racoeur, C., Jooste, V., Vey, N., Quesnel, B., Fenaux, P., Bastie, J.N., Beyne-Rauzy, O., et al.; Groupe Francophone des Myélodysplasies (2009). TET2 gene mutation is a frequent and adverse event in chronic myelomonocytic leukemia. Haematologica *94*, 1676–1681.

Lemonnier, F., Couronné, L., Parrens, M., Jaïs, J.P., Travert, M., Lamant, L., Tournillac, O., Rousset, T., Fabiani, B., Cairns, R.A., et al. (2012). Recurrent TET2 mutations in peripheral T-cell lymphomas correlate with TFH-like features and adverse clinical parameters. Blood *120*, 1466–1469.

Li, Z., Cai, X., Cai, C.L., Wang, J., Zhang, W., Petersen, B.E., Yang, F.C., and Xu, M. (2011). Deletion of Tet2 in mice leads to dysregulated hematopoietic stem cells and subsequent development of myeloid malignancies. Blood *118*, 4509–4518.

Love, M.I., Huber, W., and Anders, S. (2014). Moderated estimation of fold change and dispersion for RNA-seq data with DESeq2. Genome Biol. *15*, 550.

Moran-Crusio, K., Reavie, L., Shih, A., Abdel-Wahab, O., Ndiaye-Lobry, D., Lobry, C., Figueroa, M.E., Vasanthakumar, A., Patel, J., Zhao, X., et al. (2011). Tet2 loss leads to increased hematopoietic stem cell self-renewal and myeloid transformation. Cancer Cell *20*, 11–24.

Mouly, E., Ghamlouch, H., Della-Valle, V., Scourzic, L., Quivoron, C., Roos-Weil, D., Pawlikowska, P., Saada, V., Diop, M.K., Lopez, C.K., et al. (2018). B-cell tumor development in *Tet2*-deficient mice. Blood Adv. *2*, 703–714.

Pan, F., Wingo, T.S., Zhao, Z., Gao, R., Makishima, H., Qu, G., Lin, L., Yu, M., Ortega, J.R., Wang, J., et al. (2017). Tet2 loss leads to hypermutagenicity in haematopoietic stem/progenitor cells. Nat. Commun. *8*, 15102.

Purton, L.E., and Scadden, D.T. (2007). Limiting factors in murine hematopoietic stem cell assays. Cell Stem Cell *1*, 263–270.

Quivoron, C., Couronné, L., Della Valle, V., Lopez, C.K., Plo, I., Wagner-Ballon, O., Do Cruzeiro, M., Delhommeau, F., Arnulf, B., Stern, M.H., et al. (2011). TET2 inactivation results in pleiotropic hematopoietic abnormalities in mouse and is a recurrent event during human lymphomagenesis. Cancer Cell *20*, 25–38.

Reddy, A., Zhang, J., Davis, N.S., Moffitt, A.B., Love, C.L., Waldrop, A., Leppa, S., Pasanen, A., Meriranta, L., Karjalainen-Lindsberg, M.L., et al. (2017). Genetic and functional drivers of diffuse large B cell lymphoma. Cell *171*, 481–494.e415.

Sato, H., Wheat, J.C., Steidl, U., and Ito, K. (2016). DNMT3A and TET2 in the Pre-Leukemic Phase of Hematopoietic Disorders. Front. Oncol. *6*, 187.

Schneider, C.A., Rasband, W.S., and Eliceiri, K.W. (2012). NIH Image to ImageJ: 25 years of image analysis. Nat. Methods *9*, 671–675.

Song, S.J., Ito, K., Ala, U., Kats, L., Webster, K., Sun, S.M., Jongen-Lavrencic, M., Manova-Todorova, K., Teruya-Feldstein, J., Avigan, D.E., et al. (2013). The oncogenic microRNA miR-22 targets the TET2 tumor suppressor to promote hematopoietic stem cell self-renewal and transformation. Cell Stem Cell *13*, 87–101.

Tahiliani, M., Koh, K.P., Shen, Y., Pastor, W.A., Bandukwala, H., Brudno, Y., Agarwal, S., Iyer, L.M., Liu, D.R., Aravind, L., and Rao, A. (2009). Conversion of 5-methylcytosine to 5-hydroxymethylcytosine in mammalian DNA by MLL partner TET1. Science *324*, 930–935.

Tefferi, A., and Vardiman, J.W. (2009). Myelodysplastic syndromes. N. Engl. J. Med. *361*, 1872–1885.

Trapnell, C., Williams, B.A., Pertea, G., Mortazavi, A., Kwan, G., van Baren, M.J., Salzberg, S.L., Wold, B.J., and Pachter, L. (2010). Transcript assembly and quantification by RNA-Seq reveals unannotated transcripts and isoform switching during cell differentiation. Nat. Biotechnol. *28*, 511–515.

Wang, S.A. (2011). Diagnosis of myelodysplastic syndromes in cytopenic patients. Hematol. Oncol. Clin. North Am. *25*, 1085–1110, vii.

Wang, H., Yang, H., Shivalila, C.S., Dawlaty, M.M., Cheng, A.W., Zhang, F., and Jaenisch, R. (2013). One-step generation of mice carrying mutations in multiple genes by CRISPR/Cas-mediated genome engineering. Cell *153*, 910–918.

Williams, K., Christensen, J., Pedersen, M.T., Johansen, J.V., Cloos, P.A., Rappsilber, J., and Helin, K. (2011). TET1 and hydroxymethylcytosine in transcription and DNA methylation fidelity. Nature *473*, 343–348.

Wu, H., D'Alessio, A.C., Ito, S., Xia, K., Wang, Z., Cui, K., Zhao, K., Sun, Y.E., and Zhang, Y. (2011). Dual functions of Tet1 in transcriptional regulation in mouse embryonic stem cells. Nature *473*, 389–393.

Yu, E.M., Kittai, A., and Tabbara, I.A. (2015). Chronic lymphocytic leukemia: current concepts. Anticancer Res. *35*, 5149–5165.

Zhang, Q., Zhao, K., Shen, Q., Han, Y., Gu, Y., Li, X., Zhao, D., Liu, Y., Wang, C., Zhang, X., et al. (2015). Tet2 is required to resolve inflammation by recruiting Hdac2 to specifically repress IL-6. Nature *525*, 389–393.

STAR★METHODS

KEY RESOURCES TABLE

REAGENT or RESOURCE	SOURCE	IDENTIFIER
Antibodies		
Anti-Tet2	Abcam	Cat# ab124297; RRID: AB_2722695
Anti-Actin	Abcam	Cat# AC-15; RRID: AB_1658432
Anti-5hmC	Active Motif	Cat# 39770; RRID: AB_10013602
Goat Anti-Rabbit IgG-HRP	CalBiochem	Cat# 401393-2ML; RRID: AB_437797
Goat Anti-Mouse IgG-HRP	CalBiochem	Cat# 401253; RRID: AB_437779
CD4 (GK1.5)	BD Bioscience	Cat# 553728; RRID: AB_395012
B220 (RA3-6B2)	BD Bioscience	Cat# 553086; RRID: AB_394616
TER-119 (TER-119)	BD Bioscience	Cat# 553672; RRID: AB_394985
CD11b (M1/70)	BD Bioscience	Cat# 553309; RRID: AB_394773
CD19 (1D3)	BD Bioscience	Cat# 553784; RRID: AB_395048
CD43 (S7)	BD Bioscience	Cat# 560663; RRID: AB_1727479
NK-1.1 (PK136)	BD Bioscience	Cat# 553163; RRID: AB_394675
c-Kit (2B8)	BioLegend	Cat# 105826; RRID: AB_1626278
Gr-1 (RB6-8C5)	BioLegend	Cat# 108404; RRID: AB_313369
CD135 (A2F10)	eBiosciences	Cat# 12-1351-82; RRID: AB_465859
CD34 (RAM34)	eBiosciences	Cat# 11-0341-85; RRID: AB_465022
Sca-1 (D7)	eBiosciences	Cat# 25-5981-81; RRID: AB_469668
CD3e (145-2C11)	eBiosciences	Cat# 13-0031-85; RRID: AB_466320
CD8 (53-6.72)	eBiosciences	Cat# 13-0081-85; RRID: AB_466347
IgM (II/41)	eBiosciences	Cat# 13-5790-85; RRID: AB_466676
CD71 (R17217)	eBiosciences	Cat# 11-0711-82; RRID: AB_465124
CD127 (A7R34)	eBiosciences	Cat# 12-1271-82; RRID: AB_465844
CD45.2 or Ly5.2 (104)	eBiosciences	Cat# 11-0454-82; RRID: AB_465061
CD45.1 or Ly5.1 (A20)	eBiosciences	Cat# 25-0453-81; RRID: AB_469628
Streptavidin-APC-eFluor780	eBiosciences	Cat# 47-4317-82; RRID: AB_10366688
Streptavidin-PerCP-Cy5.5	eBiosciences	Cat# 45-4317-82; RRID: AB_10311495
Critical Commercial Assays		
RNAeasy Mini kit	QIAGEN	74104
Superscript III first strand	Invitrogen	18080-400
XtremeGene 9 DNA transfection reagent	Roche	06365787001
Deposited Data		
RNA-seq data	This paper	GEO: GSE132090
Experimental Models: Organisms/Strains		
Tet2 $^{-/-}$ (Tet2 KO) mouse	Li et al., 2011	N.A.
Tet2 $^{m/m}$ (Tet2 Mut) mouse	This paper	N.A.
B6.SJL-Ptprca Pepcb/BoyJ	Jackson lab	002014
Oligonucleotides		
RT-qPCR primers, see Table S1	This paper	n/a
Genotyping Primers, see Table S1	This paper	n/a
gRNA oligos for gene targeting, see Table S1	This paper	n/a
Recombinant DNA		
Topo pcr2.1 donor vector	This paper	n/a
pX330-Tet2-gRNA	This paper	n/a
FUW-ires-puro	This paper	n/a

(*Continued on next page*)

Continued		
REAGENT or RESOURCE	SOURCE	IDENTIFIER
FUW-HA-mGata2-ires-puro	This paper	n/a
Software and Algorithms		
Trim galore v0.4.1	Github	https://github.com/FelixKrueger/TrimGalore
Tophat v2.0.13	John Hopkins University	https://ccb.jhu.edu/software/tophat/index.shtml
HTSeq v0.6.1	Anders et al., 2015	https://github.com/simon-anders/htseq
Cufflinks v2.2	Trapnell et al., 2010	http://cole-trapnell-lab.github.io/cufflinks/
DESeq2 v1.20.0	Love et al., 2014	http://www.bioconductor.org/packages/release/bioc/html/DESeq2.html
DAVID 6.8	Jiao et al., 2012	https://david.ncifcrf.gov/
GraphPad Prism 7	GraphPad	https://www.graphpad.com/
ImageJ	Schneider et al., 2012	https://imagej.nih.gov/ij/

LEAD CONTACT AND MATERIALS AVAILABILITY

This study did not generate new unique reagents. Further information and requests for resources and reagents (including mouse strains, cell lines and plasmids generated in this study) should be directed to and will be fulfilled by the Lead Contact, Ke.I. (keisuke.ito@einstein.yu.edu).

EXPERIMENTAL MODEL AND SUBJECT DETAILS

A gene block carrying nucleotide substitutions in *Tet2* exon 9 to introduce point mutations H1367Y and D1369A into the enzymatic pocket of Tet2 was synthesized (Table S1) and cloned into Topo PCR2.1 vector. This donor plasmid along with a pX330 plasmid expressing Cas9 and a gRNA against *Tet2* exon 9 (Table S1) were used for gene editing in V6.5 mESCs (background: mixed 129/B6, sex: male) following our previously published protocols (Wang et al., 2013). These mutations only changed the conserved HRD amino acids in the iron-binding site of the catalytic domain to YRA. They are shown to render the enzyme catalytically inactive without compromising the stability or localization of Tet2, and *in vitro* biochemical and *in vivo* overexpression systems have confirmed their lack of activity on methylated DNA (Ito et al., 2010; Tahiliani et al., 2009). Targeted clones were screened by RFLP (restriction fragment length polymorphism) using a unique HaeIII restriction site introduced with silent mutations in the *Tet2* mutant allele. Properly edited clones were verified by Sanger sequencing. A heterozygote $Tet2^{+/m}$ ESC clone was injected into mouse blastocysts at the Einstein Transgenic Core facility. Chimeric animals were bred to wild-type mice to obtain $Tet2^{m/m}$ (Mut) mice. $Tet2^{-/-}$ (KO) mice, published previously (Li et al., 2011), were obtained from Dr. Mingjing Xu (University of Maimi). *Tet2* KO and *Tet2* Mut mice were intercrossed to avoid any variations due to background differences between the different groups. Cohorts of $Tet2^{+/+}$ (wild-type), *Tet2* KO and *Tet2* Mut mice (consisting of equal number of male and female animals in each group) were established and housed in an SPF (Specific-pathogen-free) barrier facility. All animals in this study included both sexes and were in a mixed 129/B6 background. Animals were examined weekly for distended belly, enlarged lymph nodes and spleen, overall mobility, and health. The peripheral blood of moribund animals was collected for analysis. Moribund animals were scarified and hematopoietic tissues including spleen, lymph nodes and bone marrow were subjected to further histological and flow cytometric evaluation to characterize the disease. All studies were performed in accordance with our IACUC approved protocols overseen by the Institute for Animal Studies at Albert Einstein College of Medicine.

METHOD DETAILS

5hmC quantification

DNA was isolated from total bone marrow of 3-month-old mice and analyzed by dot blot using anti 5hmC antibody (Active Motif) following manufacturer protocol. Breifly, DNA was spotted in replicates on Hybond N^+ membranes, dried at room temperature, blocked in 5% milk and then probed with anti 5hmC antibody (Active Motif 1:10,000) for 1hr followed by three 10min washes in PBST. Membrane was probed with secondary HRP-conjugated anti rabbit antibody (1:500) for 1hr and washed three times with PBST before developing using ECL western blot detection reagent and autoradiogrpahy. 5hmC signal intensity was quantified by ImageJ software (Schneider et al., 2012) and plotted as the average of three independent experiments.

Western blot

Bone marrow from 4-month-old mice was isolated, lysed with laemmmli sample buffer, and boiled. Lysates were resolved on 6%–10% SDS-PAGE (Mini-PROTEAN electrophoresis chamber, Bio-Rad), and transferred on PVDF membranes (Mini Trans-Blot

apparatus, Bio-Rad) following manufacturer's protocols. Membranes were blocked in 5% milk in PBS with 0.1% tween (PBST) and incubated overnight at 4°C, or for 1hr at room temperature with primary antibodies (Tet2 ab124297, abcam 1:1000, and Actin AC-15, abcam 1:40000). Secondary antibody incubations (HRP-anti mouse, 401253, or anti rabbit, 401393, 1:5000, CalBiochem) were carried out for 1hr at room temperature. Protien signal was detected using ECL western blot detection reagent and autoradiogrpahy. Protein signal intensity was quantified by ImageJ. Tet2 signal was normalized to actin signal.

Flow cytometry

For flow cytometric analyses, we used monoclonal antibodies specific for the following: CD135 (A2F10), CD34 (RAM34), Sca-1 (D7), CD3e (145-2C11), CD8 (53-6.72), IgM (II/41), F4/80 (BM8), CD71 (R17217), CD127 (A7R34), CD23 (B3B4), CD24 (M1/69), CD45.2 or Ly5.2 (104), and CD45.1 or Ly5.1 (A20); all were from eBioscience. CD4 (GK1.5), B220 (RA3-6B2), TER-119 (TER-119), CD11b (M1/70), CD19 (1D3), CD43 (S7) and NK-1.1 (PK136) were from BD Bioscience. CD150 (TC15-12F12.2), CD48 (HM48-1), c-Kit (2B8) and Gr-1 (RB6-8C5) were from BioLegend. A mixture of monoclonal antibodies against CD4, CD8, CD3e, B220, TER-119, CD11b, Gr-1, IgM, CD19, CD127, and NK-1.1 was used as a lineage marker (Lineage). When CLL was assessed, the antibody against CD127 was not included in the lineage mixture. In some experiments, Streptavidin-APC-eFluor 780 (47-4317) or -PerCP-Cy5.5 (45-4317) was used as a secondary antibody.

Colony formation assay

The colony formation assay was performed using MethoCult GF M3434 (Stem Cell Technologies, Vancouver, BC, Canada) according to the manufacturer's instructions. Briefly, the flow sorted $Lin^{-}Sca\text{-}1^{+}c\text{-}Kit^{+}$ cells (500 cells/plate, triplicate culture) were seeded into methylcellulose-based medium, and colonies were counted under microscope after 7 days incubation at $37C^{o}$, 5% CO_2. GEMM, Colony-forming unit-granulocyte, erythroid, macrophage, and megakaryocyte; GM, Colony-forming unit-granulocyte and macrophage; M, Colony-forming unit-macrophage; E, Burst-forming unit-erythroid. Long-term cultures and *in vitro* replating assay was performed as previously reported (500 $Lin^{-}Sca\text{-}1^{+}c\text{-}Kit^{+}$ cells/replicate, triplicate culture) (Ito et al., 2012; Ito et al., 2016; Song et al., 2013). Frequencies of cells with colony forming capacity after long-term *in vitro* culture were calculated using a limiting-dilution method (maximum likelihood from the proportion of negative wells measured for each input dilution of cells tested) (Purton and Scadden, 2007). In each experiment, at least 12 replicates of each dilution were performed, and a split-plot analysis of variance was used to investigate the difference between the two conditions.

Analysis of hematopoiesis

The collected peripheral blood was smeared for May-Grünwald-Giemsa staining, and/or subjected to an automated blood count. In some cases, hematological organs, including bone marrows and spleens, were sampled and subjected to evaluate the infiltration of the hematological disorders. To determine the *in vivo* transplantability of the disease, 1.0×10^5 bone marrow mononuclear cells (BMMNCs) from primary deceased *Tet2* Mut, *Tet* KO mice or littermate controls (Ly5.2) were transplanted into irradiated recipient mice (Ly5.1) with 4.0×10^5 competitor BMMNCs (Ly5.1/2). Donor (Ly5.2) cells were reconstituted. Repopulation of donor myeloid and lymphoid cells were monitored, and in some experiments, donor contribution to the immature hematopoietic lineages also evaluated.

Gene expression profiling by RNA-seq analysis

LSK and Lin^{-} cells were sorted from pooled bone marrow of two 10-week-old mice and RNA was extracted using QIAGEN RNAeasy Kit. RNA was amplified and barcoded and used to prepare libraries of two technical replicates, with ERCC spike in controls. The libraries were subjected to 150bp paired-end sequencing (Illumina HiSeq 2500 platform) at the Einstein Epigenomics core. This generated 15∼40 million read pairs per sample. The reads were trimmed using the TrimGalore (v 0.4.1, https://github.com/FelixKrueger/TrimGalore) to remove adaptors and then mapped to the mouse genome (mm10) by TopHat2 software (v 2.0.13) with default parameters (Kim et al., 2013). The read pair numbers mapped to individual genes in the Refseq gene annotation (downloaded from the UCSC genome browser in 03/2017) were calculated with the software HTseq (v 0.6.1) (Anders et al., 2015) using "–s reverse" parameter. The Fragments Per Kilobase of transcript per Million (FPKMs) were calculated using the Cufflinks package (v 2.2.1) (Trapnell et al., 2010). Read counts at the genes with FPKM > 1 were determined by the DESeq2 software (Love et al., 2014) for differential expression. False Discovery Rate (FDR) < 0.05 was used for selecting differentially expressed genes (DEGs) between *Tet2* Mut and wild-type or *Tet2* KO and wild-type samples. Gene Ontology (GO) analysis was performed by DAVID (Jiao et al., 2012) (https://david.ncifcrf.gov/tools.jsp). Bubble plots were used to show enriched GO terms and KEGG pathways. In the bubble plots, enrichment factors were calculated as the ratio of gene counts that mapped to a certain pathway versus the total gene number of that pathway. The expression patterns of the combined DEGS were identified by hierarchical clustering and displayed as heatmap. Tet2 ChIP-seq peaks were obtained from a previous study of bone morrow (Deplus et al., 2013). They were first converted to the mm10 version using the LiftOver tool from the UCSC genome browser, and then associated to genes and separated into promoter peaks (< +/− 2kb of transcription start sites; TSSs), gene body peaks, or distal regulatory peaks (< +/−50 kb of start and end of genes). Genes associated with Tet2 peaks were considered as Tet2 bound genes and compared to the list of DEGs. The RNA-seq gene expression datasets have been deposited in the Gene Expression Omnibus database.

RT-qPCR

RNA from LSK or Lin$^-$ cells sorted from two-month-old mouse bone marrow was isolated using Qaigen RNAeasy Kit and subjected to cDNA synthesis using Superscript III First-Strand synthesis system, Invitrogen. Real time quantitative PCR was performed using SYBR green master mix (Applied Biosystems) in QunatStudio 6 Flex Real-Time PCR system following standard protocols. Relative gene expression level was analyzed by comparative Ct method and was normalized to Gapdh. Primer sequences for all genes are shown in supplemental information (Table S1).

Gata2 lentiviral preparation and transduction of bone marrow

HA-tagged mouse Gata2 was cloned into FUW-ires-Puro vector. Lentivirus was prepared by transfecting FUW-HA-mGata2 or empty vector into HEK293T cells along with viral packing plasmids (pPAX2 and pMDG) using X-tremeGENE DNA transfection reagent (Roche) following manufacturer's protocol. Media was refreshed after 16hrs. Viral soup was harvested 24hr and 48hr later. Bone marrow isolated from moribund mice was cultured, transduced for 24hrs and then selected for 24hrs in puromycin (1ug/mL). Selected cells were subjected to hematopoietic analyses by FACS and transplantation studies as explained above.

QUANTIFICATION AND STATISTICAL ANALYSES

Data were processed and analyzed in Graphpad PRISM software. Log rank, one-way ANOVA and Student t test were utilized to determine statistical significance unless otherwise specified. *P*-values lower than 0.05 were considered statistically significant. Statistical methods for analysis of genome wide datasets involving RNA-seq are explained in detail under the respective sections as part of the detailed methods.

DATA AND CODE AVAILABILITY

The RNA-seq datasets have been deposited in the Gene Expression Omnibus (GEO) database (Accession number GSE132090). Mouse strains, cell lines and plasmids generated in this study will be made available upon request.

Cell Reports, Volume *28*

Supplemental Information

Non-catalytic Roles of Tet2 Are Essential to Regulate Hematopoietic Stem and Progenitor Cell Homeostasis

Kyoko Ito, Joun Lee, Stephanie Chrysanthou, Yilin Zhao, Katherine Josephs, Hiroyo Sato, Julie Teruya-Feldstein, Deyou Zheng, Meelad M. Dawlaty, and Keisuke Ito

Figure S1

A

Tet2 targeting in V6.5 mESCs	
mESCs colonies picked & screened	96
Clones heterozygote for *m* allele (*+/m*)	6
+/m clones with non-intact *wt* allele	4
Efficiency of proper targeting (2 out of 96)	2%

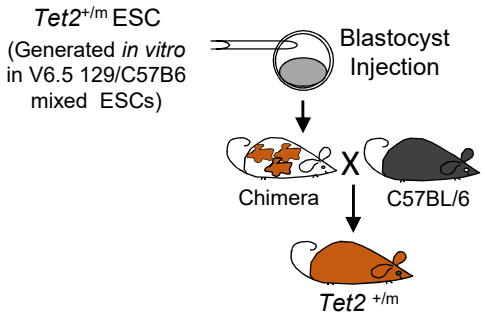

B

Tet2$^{m/m}$ mice from *Tet2*$^{+/m}$ X *Tet2*$^{+/m}$ cross

No. of Pups	+/+	+/m	m/m
65 (10 litters)	20	30	15
Percent (ratio)	30 (1)	46 (2)	23 (1)

Tet2$^{-/-}$ mice from *Tet2*$^{+/-}$ X *Tet2*$^{+/-}$ cross

No. of Pups	+/+	+/–	–/–
79 (10 litters)	23	34	22
Percent (ratio)	29 (1)	43 (2)	27 (1)

C

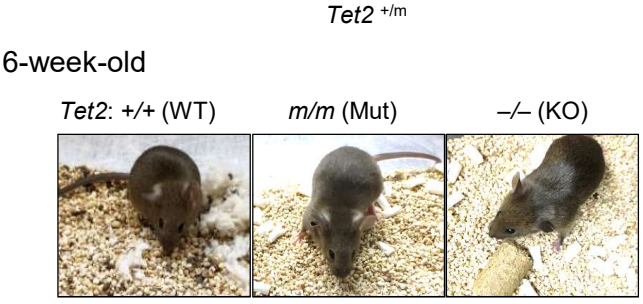

D

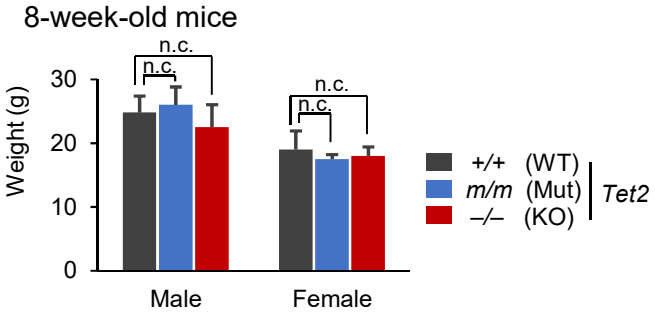

E

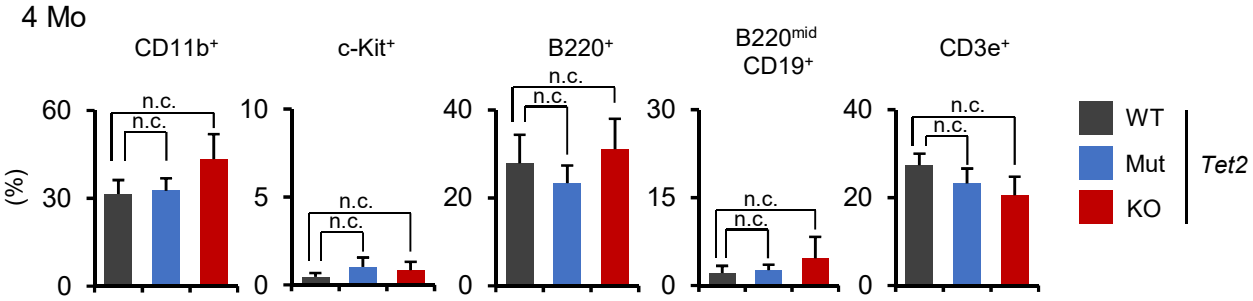

F

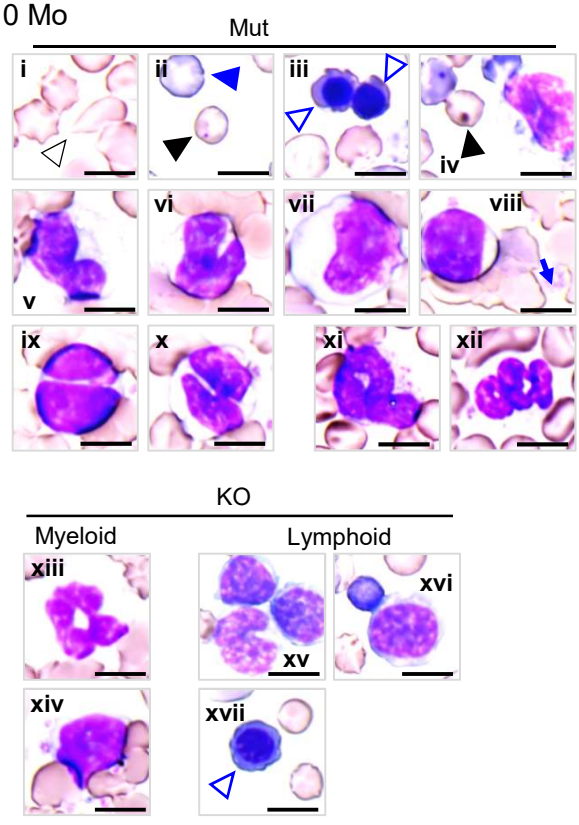

G

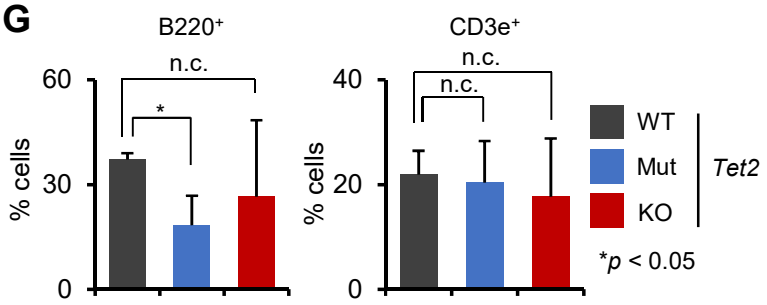

H

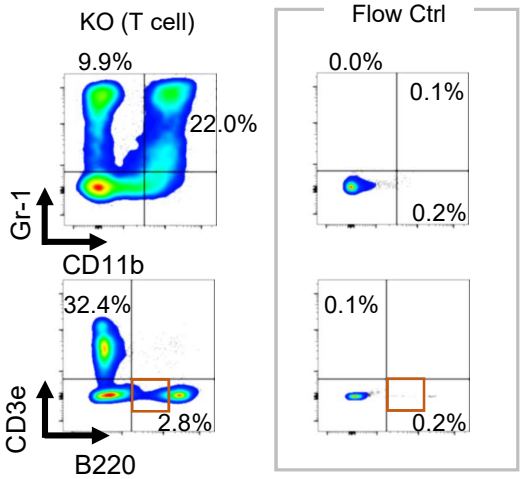

Figure S1 (Related to Figure 1). Generation and hematopoietic characterization of *Tet2* catalytic mutant mice

(A) Summary of *Tet2* gene-editing in mouse ES cells (top) and schematic of injection of an edited ESC clone into blastocyst to generate *Tet2* catalytic mutant mice.

(B) Mendelian ratios of *Tet2* catalytic mutant (Mut) and knockout (KO) mice. *Tet2* Mut mice, like knockout mice, are produced at normal mendelian frequency.

(C) Images of 6-week-old *Tet2* mice of the indicated genotypes.

(D) Body weight of live *Tet2* Mut and KO mice showing no differences in overall growth in young age.

(E) Percentages of the indicated fractions in the peripheral blood in *Tet2* Mut and KO mice (4 months old) (n = 6).

(F) Representative images of abnormal hematopoietic cells in PB smears of 10-month-old *Tet2* Mut (i-xii) and KO mice (xiii-xiv, with myeloid disorders; xv-xvii, with lymphoid malignancy). Dysplastic erythroid cells [i-iv, xvii; polychromatophilic (ii, blue arrowhead), Howell-Jolly bodies (ii and iv, black arrowhead), other poikilocytes (e.g. teardrop-shaped dacrocyte and echinocytes) (i, black-outlined arrowhead), and nucleated erythroid cells (iii and xvii, blue-outlined arrowhead). Dysplastic monocytes [v-x and xiv; a peudo-Pelger-Huet anomaly (ix and x)] and dysplastic platelet (giant platelet) (blue arrow, viii) are shown. Dysplastic neutrophils (xi-xiii) and immature B cells (xv and xvi) are also shown. All images are taken at x100. Scale bars, 10μm.

(G) Percentages of $B220^{+}$ (left) and $CD3e^{+}$ (middle) cells in the PB in *Tet2* Mut and KO mice (10 months old).

(H) Representative flow data for myeloid and lymphoid lineages in PB from *Tet2* KO mice with T lymphoid phenotypes (10 months old). Unstained flow controls are also shown (right, inset).

Error bars indicate standard deviation. n.c. stands for no significant change.

Figure S2

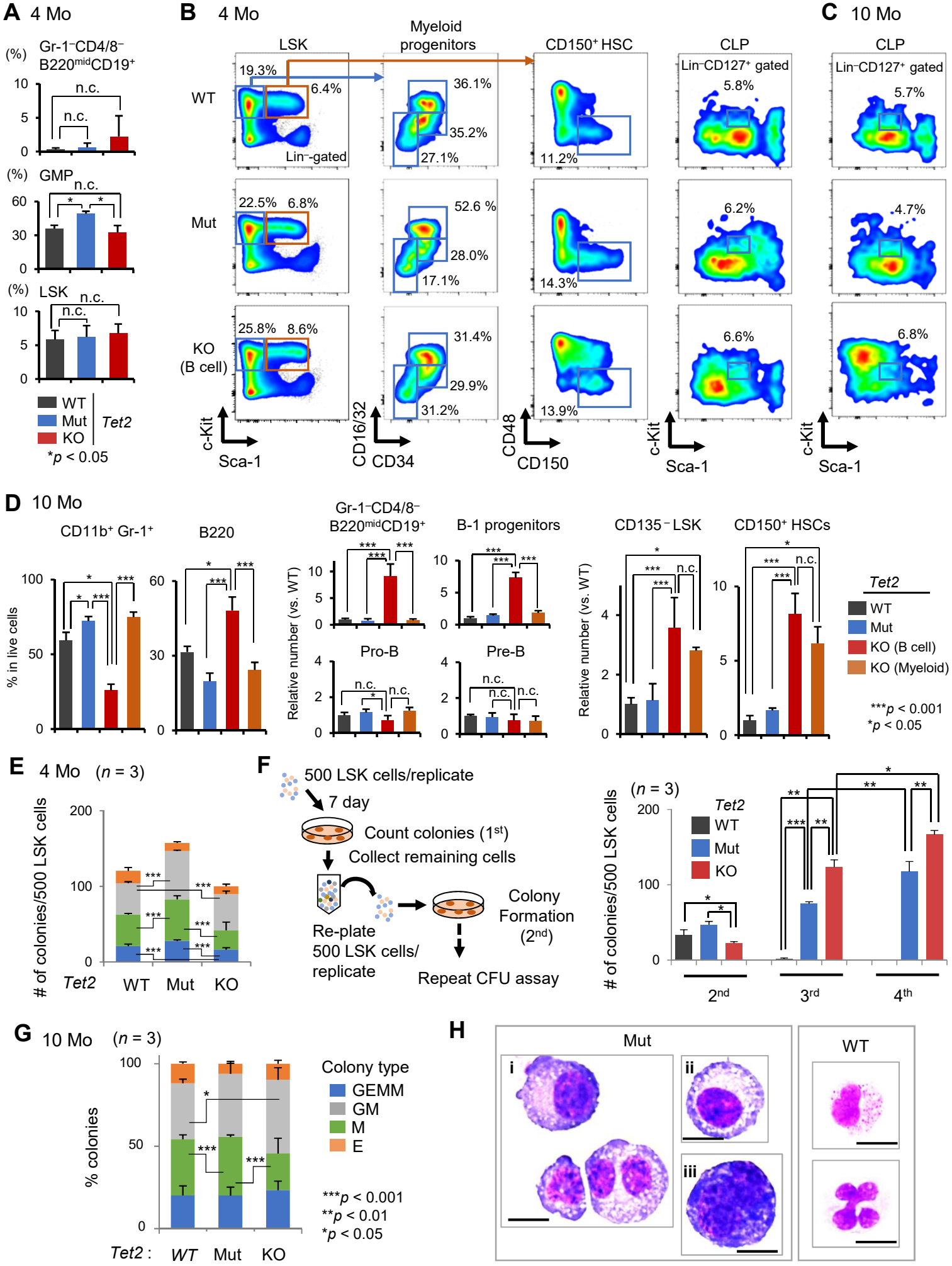
A 4 Mo
(%) Gr-1⁻CD4/8⁻ B220^mid CD19⁺
n.c.
n.c.
(%) GMP
n.c.
*
*
(%) LSK
n.c.
n.c.
WT
Mut
KO
Tet2
*p < 0.05
B 4 Mo
LSK
Myeloid progenitors
CD150⁺ HSC
CLP
Lin⁻CD127⁺ gated
WT
Mut
KO (B cell)
19.3%
6.4%
Lin⁻-gated
36.1%
35.2%
27.1%
11.2%
5.8%
22.5%
6.8%
52.6 %
28.0%
17.1%
14.3%
6.2%
25.8%
8.6%
31.4%
29.9%
31.2%
13.9%
6.6%
c-Kit
Sca-1
CD16/32
CD34
CD48
CD150
C 10 Mo
CLP
Lin⁻CD127⁺ gated
5.7%
4.7%
6.8%
D 10 Mo
CD11b⁺ Gr-1⁺
B220
Gr-1⁻CD4/8⁻ B220^mid CD19⁺
B-1 progenitors
CD135⁻ LSK
CD150⁺ HSCs
% in live cells
Relative number (vs. WT)
Pro-B
Pre-B
n.c.
Tet2
WT
Mut
KO (B cell)
KO (Myeloid)
***p < 0.001
*p < 0.05
E 4 Mo (n = 3)
# of colonies/500 LSK cells
Tet2
WT
Mut
KO
F
500 LSK cells/replicate
7 day
Count colonies (1st)
Collect remaining cells
Re-plate 500 LSK cells/ replicate
Colony Formation (2nd)
Repeat CFU assay
(n = 3)
Tet2
WT
Mut
KO
2nd
3rd
4th
G 10 Mo (n = 3)
% colonies
Colony type
GEMM
GM
M
E
***p < 0.001
**p < 0.01
*p < 0.05
Tet2 :
WT
Mut
KO
H
Mut
WT
i
ii
iii

Figure S2 (Related to Figure 2). Phenotypic and functional characterization of HSPCs from *Tet2* Mut and KO mice

(A) Percentages of the indicated fractions in the peripheral blood in *Tet2* Mut and KO mice (4 months old) (*n* = 6).

(B, C) Bone marrow flow analysis for the indicated immature fractions from *Tet2* Mut and KO mice (4 months old, B; 10 months old, C).

(D) Percentages in live mononuclear cells (left) or relative absolute number (middle, right) of the indicated fractions in the bone marrow in *Tet2* Mut and KO mice (10 months old) (*n* = 6). The alterations of Pro-B and Pre-B are minor in *Tet2* KO mice, while both B-1a fractions and B-1 progenitors are increased.

(E, F) Colony-forming capacity of HSPCs from 4-month-old *Tet2* Mut and KO mice (*n* = 3) (E). Overview of the experimental design for *in vitro* colony-replating assay (F, left). *Tet2*-KO HSCs have the increased re-plating capacity compared to *Tet2*-Mut HSCs (4 months old, up to 4^{th} round re-plating data, *n* = 3) (F, right).

(G, H) Profiles of the colonies formed by HSPCs from 10-month-old *Tet2* Mut and KO mice (*n* = 3). Representative images of May-Grünwald-Giemsa–stained cytospin preparations of the formed-colonies by hematopoietic stem and progenitor cells from *Tet2* Mut and wild-type mice (at 2^{nd} replating) (H). Scale bars, 10μm.

HSPCs, hematopoietic stem and progenitor cells; LSK, Lineage$^-$cKit$^+$Sca1$^+$; GMP, granulocyte-monocyte progenitor; CLP, common lymphoid progenitor; Pro-B, Gr-1$^-$CD4/8$^-$IgM$^-$CD43$^+$; Pro-B, Gr-1$^-$CD4/8$^-$IgM$^-$CD43$^-$; B-1 progenitor, Gr-1$^-$CD4/8$^-$IgM$^-$CD19$^+$B220$^{dim/-}$; GEMM, Colony-forming unit-granulocyte, erythroid, macrophage, and megakaryocyte; GM, Colony-forming unit-granulocyte and macrophage; M, Colony-forming unit-macrophage; E, Burst-forming unit-erythroid. Error bars indicate standard deviation. n.c. stands for no significant change.

Figure S3

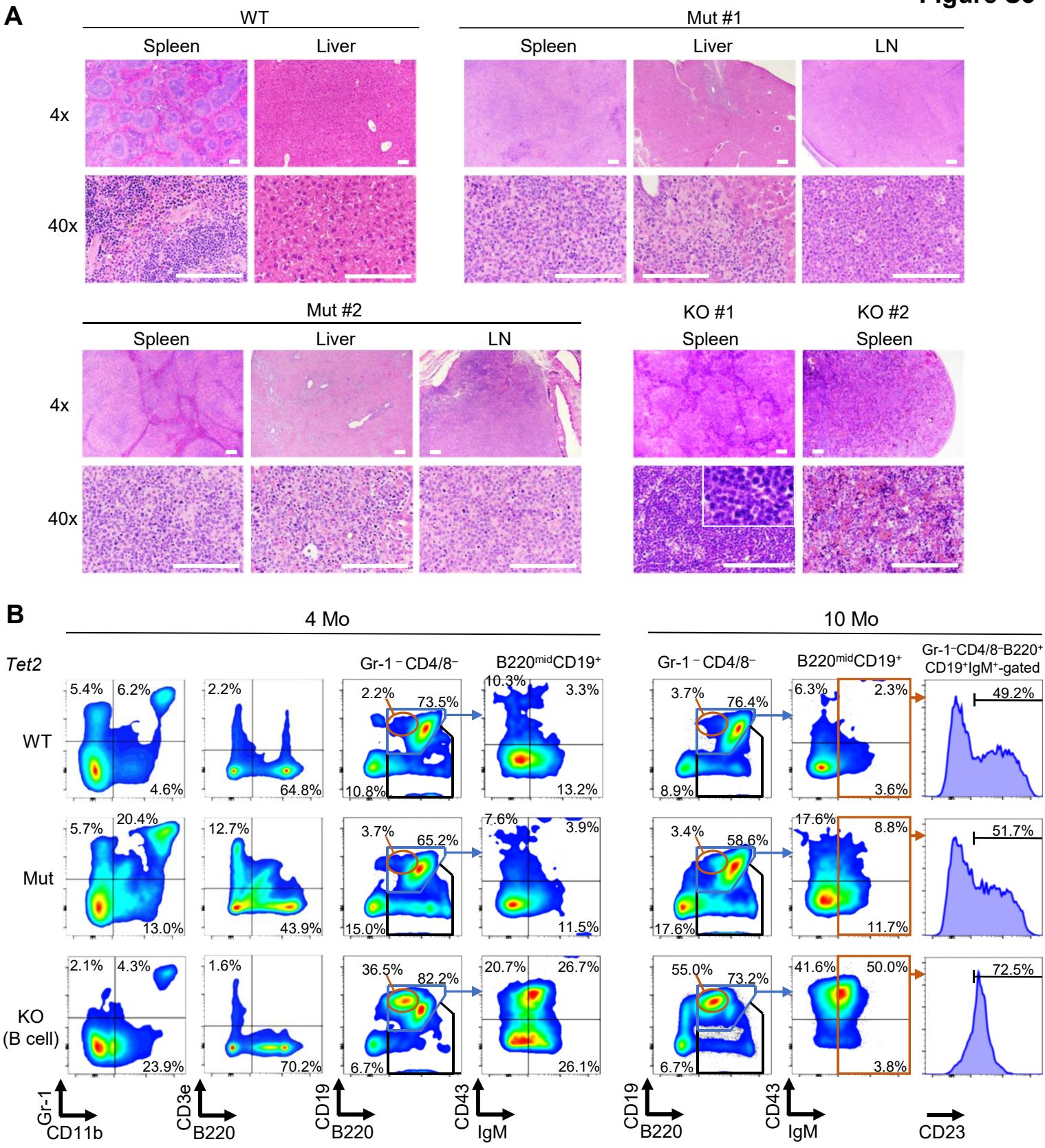
A
WT
Mut #1
Spleen
Liver
LN
4x
40x
Mut #2
KO #1
KO #2
B
4 Mo
10 Mo
Tet2
WT
Mut
KO
(B cell)
Gr-1⁻CD4/8⁻
B220midCD19+
Gr-1⁻CD4/8⁻B220+
CD19+IgM+-gated
Gr-1
CD11b
CD3e
B220
CD19
CD43
IgM
CD23
C
4 Mo
10 Mo
CD11b+
B220+
B220+ CD19+
B220mid CD19+
CD43+IgM+ in B220+CD19+
n.c.
(%)
WT
Mut
KO
Tet2
***p < 0.001
**p < 0.01
*p < 0.05

Figure S3 (Related to Figure 3). Analysis of spleens from *Tet2* Mut and KO mice

(A) Representative histologic images of sections of spleen, liver and lymph node from 10-month old *Tet2* Mut mice, stained with H&E. Tissue with myeloid expansion/infiltration are shown (top right for Mut mouse #1, and bottom left for Mut mouse #2). Histologic images of spleen from 10-month old *Tet2* KO mice with B cell phenotypes (bottom right for KO mice #1 and #2, respectively; Magnified spleen image of KO mouse #1, in the inset). Normal tissues in the age-matched wild-type mice are also shown as control (top, left). Scale bars, 250 μm.

(B, C) Representative flow data for myeloid and lymphoid lineages in the spleen from *Tet2* Mut and KO mice (4 months old, B left; 10 months old, B right). Percentages of the indicated fractions are also shown (n = 6) (C).

Error bars indicate standard deviation. n.c. stands for no significant change.

Figure S4

A

Sample ID	Total no. of reads	After TrimGalore	Trim galore	Alignment (concordant pairs)
KO-1 LSK	33177922	42%	32878550	66.2%
KO-2 LSK	24572563	46%	24353166	67.8%
Mut-1 LSK	27985348	45%	27784460	71.1%
Mut-2 LSK	29234575	45%	29026893	68.9%
WT-1 LSK	22361886	43%	22175751	63.3%
WT-2 LSK	29576940	38%	29322650	63.9%

Sample ID	Total no. of reads	After TrimGalore	Trim galore	Alignment (concordant pairs)
KO-3 Lin⁻	24823594	42%	24568085	68.7%
KO-4 Lin⁻	23783109	43%	23610520	68.3%
Mut-5 Lin⁻	41587013	28%	41206349	69.9%
Mut-6 Lin⁻	28302608	44%	28012788	68.9%
WT-1 Lin⁻	26978823	41%	26745245	67.1%
WT-2 Lin⁻	17932441	44%	17777171	70%

B

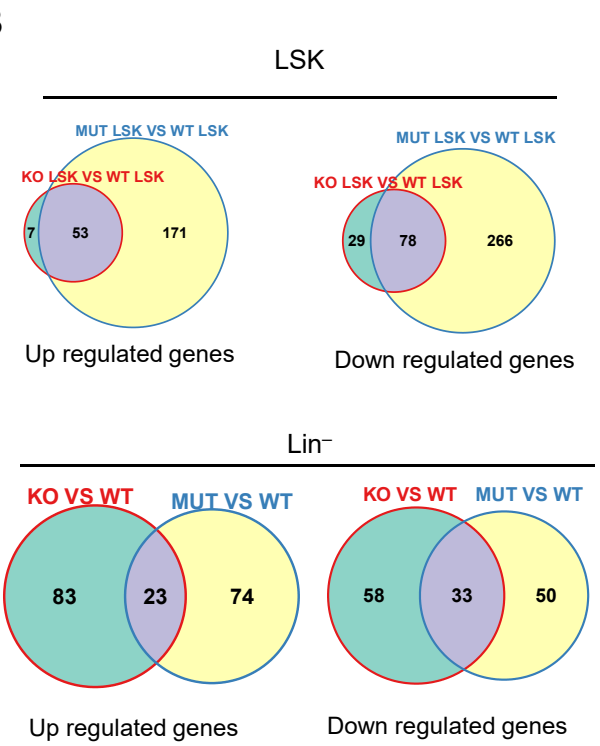

C

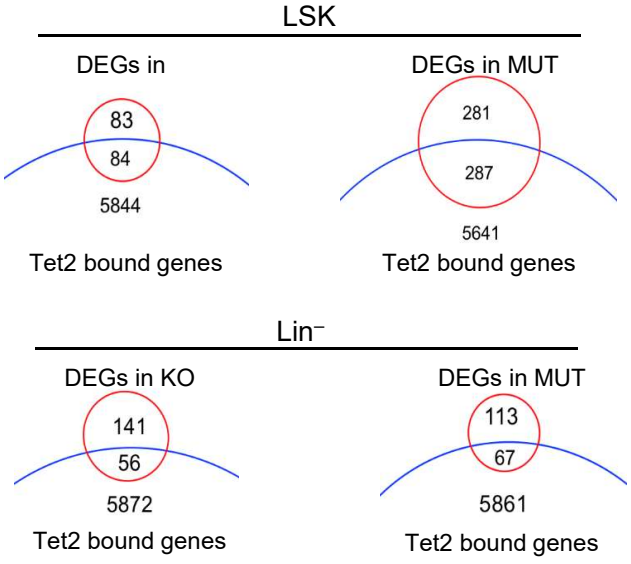

D

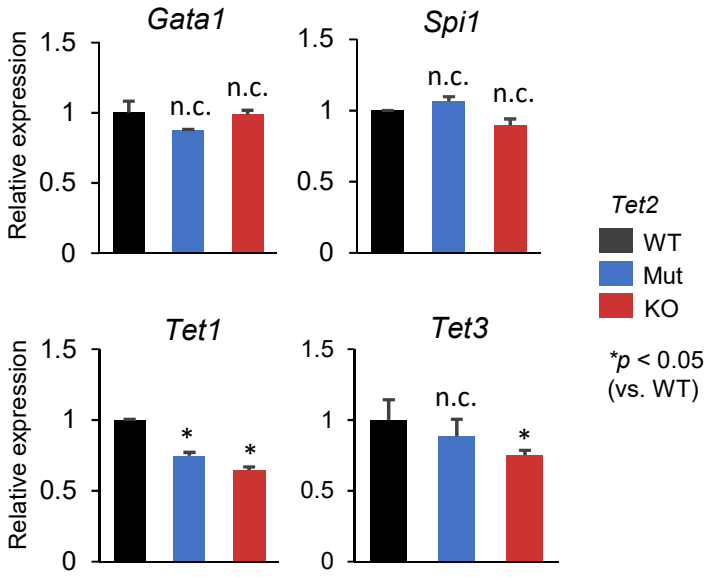

E

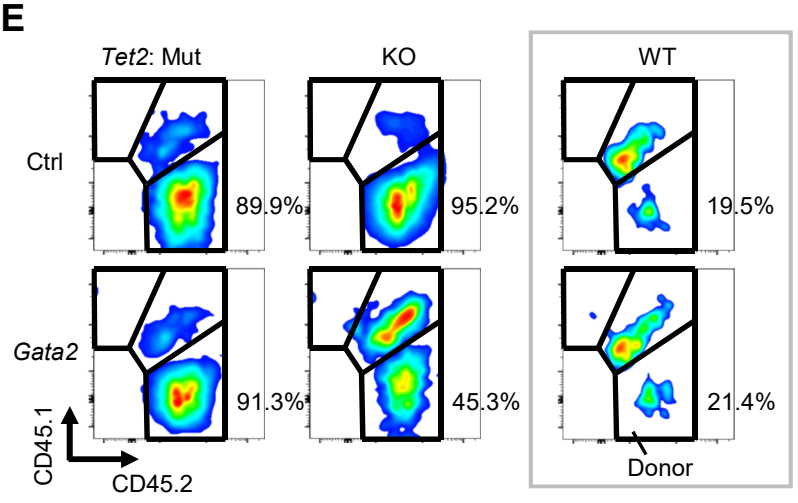

F

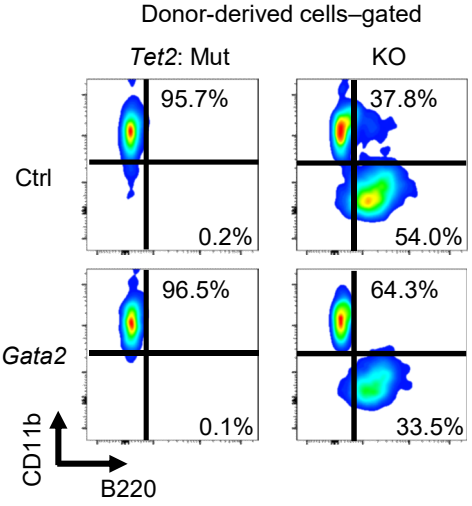

Figure S4 (Related to Figure 4): Gene expression changes in hematopoietic stem and progenitor cells from *Tet2* Mut and KO mice.

(A) Summary of RNA-seq data.

(B) Venn diagram of up- and down-regulated DEGs in LSK (left) and Lin^- cells (right).

(C) Venn diagram showing overlap of DEGs with *Tet2* bound genes in bone marrow.

(D) mRNA levels of indicated genes in LSK cells isolated from 2-month-old mice, quantified by RT-qPCR. Data normalized to *Gapdh*.

(E, F) Representative flow cytometric analysis for donor-chimerism (E) and CD11b/B220 positivity (F) in peripheral blood of recipient mice transplanted with *Gata2*-expressing *Tet2* Mut bone marrow cells (bottom left) or *Tet2* KO bone marrow cells (bottom right), 3 weeks after BMT. Empty vector transduced controls are also shown (top).

Error bars indicate standard deviation. n.c. stands for no significant change.

Table S1 (Related to STAR Methods): List of oligos, gRNAs and gene blocks used in study

Name	Sequence	Purpose	Source
Tet2 gRNA For oligo	GCATGTTCTGCTGGTCTCTG	Gene targeting	This paper
Tet2 gRNA Rev oligo	CAGAGACCAGCAGAACATGC	Gene targeting	This paper
Tet2 gene block	gcagtggttacgt… 471pb….CCTACAGGGCC…439bp ….tccatacacttaa	Gene targeting	This paper
Tet2 Mut Gen Fw	ATTCTCAGGAGTCACTGCATG	Genotyping Tet2 mutant mice	This paper
Tet2 Mut Gen Rev	TCTATCCATGAAAACACATGGCC	Genotyping Tet2 mutant mice	This paper
Tet2 KO Gen Fw	CCCATTGTTCCTTTGCTCCATGCA	Genotyping Tet2 KO mice KO allele	Zhe et al, Blood 2011
Tet2 KO Gen Rev	CGTCGCCGTCCAGCTCGACCAG	Genotyping Tet2 KO mice KO allele	Zhe et al, Blood 2011
Tet2 WT Gen Fw	CCATGCAGGGAAGACAAGAGTAGC	Genotyping Tet2 KO mice WT allele	Zhe et al, Blood 2011
Tet2 WT Gen Rev	ATCTTGTTTGGATGGAGCCCAGAG	Genotyping Tet2 KO mice WT allele	Zhe et al, Blood 2011
Tet1 RTqPCR Fw	TGCACCTACTGCAAGAATCG	Real time qPCR	Dawlaty et al, Cell Stem Cell 2011
Tet1 RTqPCR Rev	AAATTGGCATCACAGCTTCC	Real time qPCR	Dawlaty et al, Cell Stem Cell 2011
Tet2 RTqPCR Fw	GTCAACAGGACATGATCCAGGAG	Real time qPCR	Zhe et al, Blood 2011
Tet2 RTqPCR Rev	CCTGTTCCATCAGGCTTGCT	Real time qPCR	Zhe et al, Blood 2011
Tet3 RTqPCR Fw	TCCGGATTGAGAAGGTCATC	Real time qPCR	Dawlaty et al, Develop Cell 2014
Tet3 RTqPCR Rev	CCAGGCCAGGATCAAGATAA	Real time qPCR	Dawlaty et al, Develop Cell 2014
Hoxa9 RTqPCR Fw	ATGGCATTAAACCTGAACCG	Real time qPCR	Ailing et al, JCI 2013
Hoxa9 RTqPCR Rev	GTCTCCGCCGCTCTCATTC	Real time qPCR	Ailing et al, JCI 2013
Gata1 RTqPCR Fw	TGCCTGTGGCTTGTATCA	Real time qPCR	Kaimakis et al, Blood 2016
Gata1 RTqPCR Rev	TGTTGTAG GGTCGTTTGAC	Real time qPCR	Kaimakis et al, Blood 2016
Gata2 RTqPCR Fw	AAGCTGCACAATGTTAACAGG	Real time qPCR	Kaimakis et al, Blood 2016
Gata2 RTqPCR Rev	CCTTTCTTGCTCTTCTTGGAC	Real time qPCR	Kaimakis et al, Blood 2016
Gapdh RTqPCR Fw	ACATCTCACTCAAGATTGTCAGCA	Real time qPCR	Dawlaty et al, Develop Cell 2014
Gapdh RTqPCR Rev	ATGGCATGGACTGTGGTCAT	Real time qPCR	Dawlaty et al, Develop Cell 2014